

Secondary Organic Aerosol (SOA) yields from NO₃ radical + isoprene based on nighttime aircraft power plant plume transects

Juliane L. Fry¹, Steven S. Brown^{2,5}, Ann M. Middlebrook², Peter M. Edwards^{2,3,4}, Pedro Campuzano-Jost^{3,5}, Douglas A. Day^{3,5}, José L. Jimenez^{3,5}, Hannah M. Allen⁶, Thomas B. Ryerson², Ilana Pollack^{2,3,a}, Martin Graus^{3,b}, Carsten Warneke^{2,3}, Joost A. deGouw^{3,5}, Charles A. Brock², Jessica Gilman^{2,3}, Brian M. Lerner^{2,3,c}, William P. Dube^{2,3}, Jin Liao^{2,3,d}, André Welti^{2,3,e}

¹Chemistry Department, Reed College, Portland, OR, USA

²Chemical Sciences Division, Earth System Research Laboratory, National Oceanic and Atmospheric Administration, Boulder, CO, USA

³Cooperative Institute for Research in Environmental Sciences, University of Colorado, Boulder, CO, USA

⁴Wolfson Atmospheric Chemistry Laboratories, Department of Chemistry, University of York, York, UK

⁵Department of Chemistry, University of Colorado, Boulder, CO, USA

⁶Division of Chemistry and Chemical Engineering, California Institute of Technology, Pasadena, CA, USA

^anow at Department of Atmospheric Science, Colorado State University, Fort Collins, CO, USA

^bnow at Institute of Atmospheric and Cryospheric Sciences, University of Innsbruck, Austria.

^cnow at Aerodyne Research, Inc., Billerica, MA, USA

^dnow at Universities Space Research Association, Columbia, MD, USA and NASA Goddard Space Flight Center, Atmospheric Chemistry and Dynamic Laboratory, Greenbelt, MD, USA

^enow at Leibniz Institute for Tropospheric Research, Department of Physics, Leipzig, Germany

Abstract

Nighttime reaction of nitrate radicals (NO₃) with biogenic volatile organic compounds (BVOC) has been proposed as a potentially important but also highly uncertain source of secondary organic aerosol (SOA). The southeast United States has both high BVOC and nitrogen oxide (NO_x) emissions, resulting in a large model-predicted NO₃-BVOC source of SOA. Coal-fired power plants in this region constitute substantial NO_x emissions point sources into a nighttime atmosphere characterized by high regionally widespread concentrations of isoprene. In this paper, we exploit nighttime aircraft observations of these power plant plumes, in which NO₃ radicals rapidly remove isoprene, to obtain field-based estimates of the secondary organic aerosol yield from NO₃ + isoprene. Observed in-plume increases in nitrate aerosol are consistent with organic nitrate aerosol production from NO₃ + isoprene, and these are used to determine molar SOA yields, for which the average over 9 plumes is 9%. Corresponding mass yields depend on the assumed molecular formula for isoprene-NO₃-SOA, but the average over 9 plumes is 27%, larger than those previously measured in chamber studies (12 – 14% after oxidation of both double bonds). Yields are larger for longer plume ages. This suggests that ambient aging processes lead more effectively to condensable material than typical chamber conditions allow. We discuss potential mechanistic explanations for this difference, including longer ambient peroxy radical lifetimes and heterogeneous reactions of NO₃-isoprene gas phase products. More in-depth studies are needed to better understand the aerosol yield and

43 oxidation mechanism of NO₃ radical + isoprene, a coupled anthropogenic – biogenic source of
44 SOA that may be regionally significant.

45 **1 Introduction**

46 Organic aerosol (OA) is increasingly recognized as a globally important component of the fine
47 particulate matter that exerts a large but uncertain negative radiative forcing on Earth's climate
48 (Myhre et al., 2013) and adversely affects human health around the world (Lelieveld et al.,
49 2015). This global importance is complicated by large regional differences in OA concentrations
50 relative to other sources of aerosol such as black carbon, sulfate, nitrate and sea salt. OA
51 comprises 20 – 50% of total fine aerosol mass at continental mid-latitudes, but more in urban
52 environments and biomass burning plumes, and up to 90% over tropical forests (Kanakidou et
53 al., 2005, Zhang et al., 2007). Outside of urban centers and fresh biomass burning plumes, the
54 majority of this OA is secondary organic aerosol (SOA) (Jimenez et al., 2009), produced by
55 oxidation of directly emitted volatile organic compounds followed by partitioning into the aerosol
56 phase. Forests are strong biogenic VOC emitters, in the form of isoprene (C₅H₈), monoterpenes
57 (C₁₀H₁₆), and sesquiterpenes (C₁₅H₂₄), all of which are readily oxidized by the three major
58 atmospheric oxidants, OH, NO₃, and O₃. The total global source of biogenic SOA from such
59 reactions remains highly uncertain, with a review estimating it at 90 +/- 90 Tg C yr⁻¹ (Hallquist et
60 al., 2009), a large fraction of which may be anthropogenically controlled (Goldstein et al., 2009,
61 Carlton et al., 2010, Hoyle et al., 2011, Spracklen et al., 2011). As most NO₃ arises from
62 anthropogenic emissions, OA production from NO₃ + isoprene is one mechanism that could
63 allow for the anthropogenic control of biogenic SOA mass loading.

64
65 Isoprene constitutes nearly half of all global VOC emissions to the atmosphere, with a flux of
66 ~600 Tg yr⁻¹ (Guenther et al., 2006). As a result, accurate global biogenic SOA budgets depend
67 strongly on yields from isoprene oxidation. Recent global modeling efforts find that isoprene
68 SOA is produced at rates from 14 (Henze and Seinfeld 2006, Hoyle et al., 2007) to 19 TgC yr⁻¹
69 (Heald et al., 2008), which implies that it could constitute 27% (Hoyle et al., 2007) to 48%
70 (Henze and Seinfeld 2006) to 78% (Heald et al., 2008) of total SOA (based also on varying
71 estimates of total SOA burden in each study). More recent observational constraints on SOA
72 yield from isoprene find complex temperature-dependent mechanisms that could affect vertical
73 distributions (Worton et al., 2013) and suggest that isoprene SOA constitutes from 17% (Hu et
74 al., 2015) to 40% (Kim et al., 2015) up to 48% (Marais et al., 2016) of total OA in the
75 southeastern United States. This large significance comes despite isoprene's low SOA mass
76 yields – two recent observational studies estimated the total isoprene SOA mass yield to be
77 ~3% (Kim et al., 2015, Marais et al., 2016), and modeling studies typically estimate isoprene
78 SOA yields to be 4 to 10%, depending on the oxidant, in contrast to monoterpenes' yields of 10
79 to 20% and sesquiterpenes' yields of >40% (Pye et al., 2010). Furthermore, laboratory studies
80 of SOA mass yields may have a tendency to underestimate these yields, if they cannot access
81 the longer timescales of later-generation chemistry, or are otherwise run under conditions that
82 limit oxidative aging of first-generation products (Carlton et al., 2009).

83

84 Laboratory chamber studies of SOA mass yield at OA loadings of $\sim 10 \mu\text{g m}^{-3}$ from isoprene
85 have typically found low yields from O_3 (1% (Kleindienst et al., 2007)) and OH (2% at low NO_x to
86 5% at high NO_x (Kroll et al., 2006, Dommen et al., 2009); 1.3% at low NO_x and neutral seed
87 aerosol pH but rising to 29% in the presence of acidic sulfate seed aerosol due to reactive
88 uptake of epoxydiols of isoprene (IEPOX) (Surratt et al., 2010)). One recent chamber study on
89 OH-initiated isoprene SOA formation focused on the fate of second-generation RO_2 radical
90 found significantly higher yields, up to 15% at low NO_x (Liu et al., 2016), suggesting that omitting
91 later-generation oxidation chemistry could be an important limitation of early chamber
92 determinations of isoprene SOA yields. Another found an increase in SOA formed with
93 increasing HO_2 to RO_2 ratios, suggesting that RO_2 fate could also play a role in the variability of
94 previously reported SOA yields (D'Ambro et al., 2017).

95
96 For NO_3 oxidation of isoprene, early chamber experiments already pointed to higher yields (e.g.,
97 12% (Ng et al., 2008)) than for OH oxidation. Ng et al. (Ng et al., 2008) also observed chemical
98 regime differences: SOA yields were approximately two times larger when chamber conditions
99 were tuned such that first-generation peroxy radical fate was RO_2+RO_2 dominated than when it
100 was RO_2+NO_3 dominated. In addition, Rollins et al. (Rollins et al., 2009) observed a significantly
101 higher SOA yield (14%) from second-generation NO_3 oxidation than that when only one double
102 bond was oxidized (0.7%). This points to the possibility that later-generation, RO_2+RO_2
103 dominated isoprene + NO_3 chemistry may be an even more substantial source of SOA than
104 what current chamber studies have captured. Schwantes et al. (Schwantes et al., 2015)
105 investigated the gas-phase products of NO_3 + isoprene in the RO_2+HO_2 dominated regime and
106 found the major product to be isoprene nitrooxy hydroperoxide (INP, 75-78% molar yield), which
107 can photochemically convert to isoprene nitrooxy hydroxyepoxide (INHE), a molecule that might
108 contribute to SOA formation via heterogeneous uptake similar to IEPOX. Here again, multiple
109 generations of chemistry are required to produce products that may contribute to SOA.

110
111 Because the SOA yield appears to be highest for NO_3 radical oxidation, and isoprene is such an
112 abundantly emitted BVOC, oxidation of isoprene by NO_3 may be an important source of OA in
113 areas with regional NO_x pollution. Since the SOA yield with neutral aerosol seed appears to be
114 an order of magnitude larger than that from other oxidants, even if only 10% of isoprene is
115 oxidized by NO_3 , it will produce comparable SOA to daytime photo-oxidation. For example,
116 Brown et al. (Brown et al., 2009) concluded that NO_3 contributed more SOA from isoprene than
117 OH over New England, where $> 20\%$ of isoprene emitted during the previous day was available
118 at sunset to undergo dark oxidation by either NO_3 or O_3 . The corresponding contribution to total
119 SOA mass loading was 1 – 17% based on laboratory yields (Ng et al., 2017). Rollins et al.
120 (Rollins et al., 2012) concluded that multi-generational NO_3 oxidation of biogenic precursors was
121 responsible for one-third of nighttime organic aerosol increases during the CalNex-2010
122 experiment in Bakersfield, CA. In an aircraft study near Houston, TX, Brown et al. (Brown et al.,
123 2013) observed elevated organic aerosol in the nighttime boundary layer, and correlated vertical
124 profiles of organic and nitrate aerosol in regions with rapid surface level NO_3 radical production
125 and BVOC emissions. From these observations, the authors estimated an SOA source from
126 NO_3 + BVOCs within the nocturnal boundary layer of $0.05 - 1 \mu\text{g m}^{-3} \text{h}^{-1}$. Carlton et al. (Carlton
127 et al., 2009) note the large scatter in chamber-measured SOA yields from isoprene

128 photooxidation and point throughout their review of SOA formation from isoprene to the likely
129 importance of poorly understood later generations of chemistry in explaining field observations.
130 We suggest that similar differences in multi-generational chemistry could explain the variation
131 among the (sparse) chamber and field observations of NO_3 + isoprene yields described in the
132 previous paragraph, and summarized in a recent review of NO_3 + BVOC oxidation mechanisms
133 and SOA formation (Ng et al., 2017).

134
135 The initial products of NO_3 + isoprene include organic nitrates, some of which will partially
136 partition to the aerosol phase. Organic nitrates in the particle phase (pRONO_2) are challenging
137 to quantify with online methods, due to both interferences and their often overall low
138 concentrations in ambient aerosol. Hence, field datasets to constrain modeled pRONO_2 are
139 sparse (Fisher et al., 2016, Ng et al., 2017). One of the most used methods in recent studies,
140 used also here, is quantification with the Aerodyne Aerosol Mass Spectrometer (AMS). Organic
141 nitrates thermally decompose in the AMS vaporizer and different approaches have been used to
142 apportion the organic fraction contributing to the total nitrate signal. Allan et al. (Allan et al.,
143 2004) first proposed the use of nitrate peaks at m/z 30 and 46 to distinguish various nitrate
144 species with the AMS. Marcolli et al. (Marcolli et al., 2006), in the first reported tentative
145 assignment of aerosol organic nitrate using AMS data, used cluster analysis to analyze data
146 from the 2002 New England Air Quality Study. In that study, cluster analysis identified two
147 categories with high m/z 30 contributions. One of these peaked in the morning when NO_x was
148 abundant and was more prevalent in plumes with lowest photochemical ages, potentially from
149 isoprene oxidation products. The second was observed throughout the diurnal cycle in both
150 fresh and aged plumes, and contained substantial m/z 44 contribution (highly oxidized OA). A
151 subsequent AMS laboratory and field study discussed and further developed methods for
152 separate quantification of organic nitrate (in contrast to inorganic nitrate) (Farmer et al., 2010). A
153 refined version of one of these separation methods, based on the differing $\text{NO}_2^+/\text{NO}^+$
154 fragmentation ratio for organic vs. inorganic nitrate, was later employed to quantify organic
155 nitrate aerosol at two forested rural field sites where strong biogenic VOC emissions and
156 relatively low NO_x combined to make substantial organic nitrate aerosol concentrations ((Fry et
157 al., 2013, Ayres et al., 2015)). Most recently, Kiendler-Scharr et al. (Kiendler-Scharr et al., 2016)
158 used a variant of this method to conclude that across Europe, organic nitrates comprise ~40%
159 of submicron organic aerosol. Modeling analysis concluded that a substantial fraction of this
160 organic nitrate aerosol is produced via NO_3 radical initiated chemistry. Chamber studies have
161 employed this fragmentation ratio method to quantify organic nitrates (Fry et al., 2009, Rollins et
162 al., 2009, Bruns et al., 2010, Fry et al., 2011, Boyd et al., 2015), providing the beginnings of a
163 database of typical organonitrate fragmentation ratios from various BVOC precursors.

164
165 Measurements conducted at the SOAS ground site in Centreville, Alabama in 2013 found
166 evidence of significant organonitrate contribution to SOA mass loading. Xu et al. (2015) reported
167 that organic nitrates constituted 5 to 12% of total organic aerosol mass from AMS data applying
168 a variant of the $\text{NO}_2^+/\text{NO}^+$ ratio method. They identify a nighttime-peaking “LO-OOA” AMS factor
169 which they attribute to mostly NO_3 oxidation of BVOC (in addition to O_3 + BVOC). They
170 estimated that the NO_3 radical oxidizes 17% of isoprene, 20% of α -pinene, and 38% of β -pinene
171 in the nocturnal boundary layer at this site. However, applying laboratory-based SOA yields to

172 model the predicted increase in OA, Xu et al. predict only $0.7 \mu\text{g m}^{-3}$ of SOA would be
173 produced, substantially lower than the measured nighttime LO-OOA production of $1.7 \mu\text{g m}^{-3}$.
174 The more recent analysis of Zhang et al. (Zhang et al., 2018) found a strong correlation of
175 monoterpene SOA with the fraction of monoterpene oxidation attributed to NO_3 , even for non-
176 nitrate containing aerosol, suggesting an influence of NO_3 even in pathways that ultimately
177 eliminate the nitrate functionality from the SOA, such as hydrolysis or NO_2 regeneration. Ayres
178 et al. (Ayres et al., 2015) used a correlation of overnight organonitrate aerosol buildup with
179 calculated net NO_3 + monoterpene and isoprene reactions to estimate an overall NO_3 +
180 monoterpene SOA mass yield of 40 – 80%. The factor of two range in this analysis was based
181 on two different measurements of aerosol-phase organic nitrates. These authors used similar
182 correlations to identify specific CIMS-derived molecular formulae that are likely to be NO_3 radical
183 chemistry products of isoprene and monoterpenes, and found minimal contribution of identified
184 first-generation NO_3 + isoprene products to the aerosol phase (as expected based on their
185 volatility). Lee et al. (Lee et al., 2016) detected abundant highly functionalized particle-phase
186 organic nitrates at the same site, with apparent origin both from isoprene and monoterpenes,
187 and both daytime and nighttime oxidation, and estimated their average contribution to
188 submicron organic aerosol mass to be between 3 – 8 %. For the same ground campaign,
189 Romer et al. (Romer et al., 2016) found evidence of rapid conversion from alkyl nitrates to
190 HNO_3 , with total alkyl nitrates having an average daytime lifetime of 1.7 hours.

191
192 Xie et al. (Xie et al., 2013) used a model constrained by observed alkyl nitrate correlations with
193 O_3 from the INTEX-NA/ICARTT 2004 field campaign to determine a range of isoprene nitrate
194 lifetimes between 4 and 6 hours, with 40-50% of isoprene nitrates formed by NO_3 + isoprene
195 reactions. Laboratory studies show that not all organic nitrates hydrolyze to HNO_3 equally
196 rapidly: primary and secondary organic nitrates were found to be less prone to aqueous
197 hydrolysis than tertiary organic nitrates (Darer et al., 2011, Hu et al., 2011, Boyd et al., 2015,
198 Fisher et al., 2016). This suggests that field-based estimates of the contribution of organic
199 nitrates to SOA formation could be a lower limit, if they are based on measurement of those
200 aerosol-phase nitrates. This is because if hydrolysis is rapid, releasing HNO_3 but leaving behind
201 the organic fraction in the aerosol phase, then that organic mass would not be accurately
202 accounted for as arising from nitrate chemistry. This was addressed in a recent modeling study
203 of SOAS (Pye et al., 2015) in which modeled hydrolysis products of particulate organic nitrates
204 of up to $0.8 \mu\text{g m}^{-3}$ additional aerosol mass loading in the southeast U.S. were included in the
205 estimate of change in OA due to changes in NO_x . Another recent GEOS-Chem modeling study
206 using of gas- and particle-phase organic nitrates observed during the SEAC⁴RS and SOAS
207 campaigns similarly finds RONO_2 to be a major sink of NO_x across the SEUS region (Fisher et
208 al., 2016, Lee et al., 2016).

209
210 Complementing these SOAS ground site measurements, the NOAA-led SENEX (Southeast
211 Nexus) aircraft campaign conducted 18 research flights focused in part on studying the
212 interactions between biogenic and anthropogenic emissions that form secondary pollutants
213 between 3 June and 10 July 2013 (Warneke et al., 2016). Flight instrumentation focused on
214 measurement of aerosol precursors and composition enable the present investigation of SOA
215 yields using this aircraft data set. Edwards et al. (Edwards et al., 2017) used data from the

216 SENEX night flights to evaluate the nighttime oxidation of BVOC, observing high nighttime
217 isoprene mixing ratios in the residual layer that can undergo rapid NO_3 oxidation when sufficient
218 NO_x is present. These authors suggest that past NO_x reductions may have been uncoupled
219 from OA trends due to NO_x not having been the limiting chemical species for OA production, but
220 that future reductions in NO_x may decrease OA if NO_3 oxidation of BVOC is a substantial
221 regional SOA source. Because isoprene is ubiquitous in the nighttime residual layer over the
222 southeastern United States and the NO_3 + isoprene reaction is rapid, NO_3 reaction will be
223 dominant relative to O_3 in places with anthropogenic inputs of NO_x (Edwards et al. (Edwards et
224 al., 2017) concludes that when $\text{NO}_2/\text{BVOC} > 0.5$, NO_3 oxidation will be dominant). Hence, a
225 modest NO_3 + isoprene SOA yield may constitute a regionally important OA source.

226
227 Several modeling studies have investigated the effects of changing NO_x on global and SEUS
228 SOA. Hoyle et al. (Hoyle et al., 2007) found an increase in global SOA production from 35 Tg yr⁻¹
229 to 53 Tg yr⁻¹ since preindustrial times, resulting in an increase in global annual mean SOA
230 mass loading of 51%, attributable in part to changing NO_x emissions. Zheng et al. (Zheng et al.,
231 2015) found only moderate SOA reductions from a 50% reduction in NO emissions: 0.9 – 5.6 %
232 for global NO_x or 6.4 – 12.0% for southeast US NO_x , which they attributed to buffering by
233 alternate chemical pathways and offsetting tendencies in the biogenic vs. anthropogenic SOA
234 components. In contrast, Pye et al. (Pye et al., 2015) find a 9% reduction in total organic aerosol
235 in Centreville, AL for only 25% reduction in NO_x emissions. A simple limiting-reagent analysis of
236 NO_3 + monoterpene SOA from power plant plumes across the United States found that between
237 2008 and 2011, based on EPA-reported NO_x emissions inventories, some American power
238 plants shifted to the NO_x -limited regime (from 3.5% to 11% of the power plants), and showed
239 that these newly NO_x -limited power plants were primarily in the southeastern United States (Fry
240 et al., 2015). The effect of changing NO_x on SOA burden is clearly still in need of further study.

241
242 Here, we present aircraft transects of spatially discrete NO_x plumes from electric generating
243 units (EGU), or power plants (PP), as a method to specifically isolate the influence of NO_3
244 oxidation. These plumes are concentrated and highly enriched in NO_x over a scale of only a
245 few km (Brown et al., 2012), and have nitrate radical production rates ($P(\text{NO}_3)$) 10 – 100 times
246 greater than those of background air. The rapid shift in $P(\text{NO}_3)$ allows direct comparison of air
247 masses with slow and rapid oxidation rates attributable to the nitrate radical, effectively isolating
248 the influence of this single chemical pathway in producing SOA and other oxidation products.
249 Changes in organic nitrate aerosol (pRONO_2) concentration and accompanying isoprene
250 titration enable a direct field determination of the SOA yield from NO_3 + isoprene.

251 **2 Field campaign and experimental and modeling methods**

252 The Southeast Nexus (SENEX: <http://esrl.noaa.gov/csd/projects/senex/>) campaign took place 3
253 June through 10 July 2013 as the NOAA WP-3D aircraft contribution to the larger Southeast
254 Atmospheric Study (SAS: http://www.eol.ucar.edu/field_projects/sas/), a large, coordinated
255 research effort focused on understanding natural and anthropogenic emissions, oxidation
256 chemistry and production of aerosol in the summertime atmosphere in the southeastern United
257 States. The NOAA WP-3D aircraft operated 18 research flights out of Smyrna, Tennessee,

258 carrying an instrument payload oriented towards elucidating emissions inventories and reactions
259 of atmospheric trace gases, and aerosol composition and optical properties (Warneke et al.,
260 2016). One of the major goals of the larger SAS study is to quantify the fraction of organic
261 aerosol that is anthropogenically controlled, with a particular focus on understanding how OA
262 may change in the future in response to changing anthropogenic emissions.
263

264 The subset of aircraft instrumentation employed for the present analysis of nighttime NO_3 +
265 isoprene initiated SOA production includes measurements used to determine NO_3 radical
266 production rate ($P(\text{NO}_3) = k_{\text{NO}_2+\text{O}_3}(T) [\text{NO}_2] [\text{O}_3]$), isoprene and monoterpene concentrations,
267 other trace gases for plume screening and identification, aerosol size distributions, and aerosol
268 composition. The details on the individual measurements and the overall aircraft deployment
269 goals and strategy are described in Warneke et al. (Warneke et al., 2016). Briefly, NO_2 was
270 measured by UV photolysis and gas-phase chemiluminescence (P-CL) and by cavity ringdown
271 spectroscopy, (CRDS), which agreed within 6%. O_3 was also measured by both gas-phase
272 chemiluminescence and CRDS and agreed within 8%, within the combined measurement
273 uncertainties of the instruments. Various volatile organic compounds were measured with
274 several techniques, including for the isoprene and monoterpenes of interest here, proton
275 reaction transfer mass spectrometry (PTR-MS) and canister whole air samples and post-flight
276 GC-MS analysis (iWAS/GCMS). A comparison of PTR-MS and iWAS/GCMS measurements of
277 isoprene during SENEX has high scatter due to imperfect time alignment and isoprene's high
278 variability in the boundary layer, but the slope of the intercomparison is 1.04 ((Warneke et al.,
279 2016); for more details on the VOC intercomparisons, see also Lerner et al., (Lerner et al.,
280 2017)). Acetonitrile from the PTRMS was used to screen for the influence of biomass burning.
281 Sulfur dioxide (SO_2) was used to identify emissions from coal-fired power plants. All gas-phase
282 instruments used dedicated inlets, described in detail in the supplemental information for
283 Warneke et al. (Warneke et al., 2016).
284

285 Aerosol particles were sampled downstream of a low turbulence inlet (Wilson et al., 2004), after
286 which they were dried by ram heating, size-selected by an impactor with 1 μm aerodynamic
287 diameter size cut-off, and measured by various aerosol instruments (Warneke et al., 2016). An
288 ultra-high-sensitivity aerosol sizing spectrometer (UHSAS, Particle Metrics, Inc., Boulder, CO
289 (Cai et al., 2008, Brock et al., 2011)) was used to measure the dry submicron aerosol size
290 distribution down to about 70 nm. Data for the UHSAS are reported at 1 Hz whereas AMS data
291 were recorded roughly every 10 seconds. The ambient (wet) surface areas were calculated
292 according to the procedures described in Brock et al., 2016 (Brock et al., 2016). A pressure-
293 controlled inlet (Bahreini et al., 2008) was employed to ensure that a constant mass flow rate
294 was sampled by a compact time-of-flight aerosol mass spectrometer (C-ToF-AMS) which
295 measured the non-refractory aerosol composition (Drewnick et al., 2005). The aerosol volume
296 transmitted into the AMS was calculated by applying the measured AMS lens transmission
297 curve (Bahreini et al., 2008) to the measured particle volume distributions from the UHSAS. For
298 the entire SENEX study, the mean, calculated fraction of aerosol volume behind the 1 micron
299 impactor that was transmitted through the lens into the AMS instrument was 97% (with $\pm 4\%$
300 standard deviation), indicating that most of the submicron aerosol volume measured by the
301 sizing instruments was sampled by the AMS.

302
303 After applying calibrations and the composition-dependent collection efficiency following
304 Middlebrook et al. (Middlebrook et al., 2012), the limits of detection for the flight analyzed here
305 were $0.05 \mu\text{g m}^{-3}$ for nitrate, $0.26 \mu\text{g m}^{-3}$ for organic mass, $0.21 \mu\text{g m}^{-3}$ for ammonium, and 0.05
306 $\mu\text{g m}^{-3}$ for sulfate, determined as three times the standard deviation of 10-second filtered air
307 measurements obtained for 10 minutes during preflight and 10 minutes during postflight (110
308 datapoints). Note that the relative ionization efficiency for ammonium was 3.91 and 3.87 for the
309 two bracketing calibrations and an average value of 3.9 was used for the flight analyzed here.
310 An orthogonal distance regression (ODR-2) of the volume from composition data (AMS mass
311 plus refractory black carbon) using a mass weighted density as described by Bahreini et al.
312 (Bahreini et al., 2009) versus the volume based on the sizing instruments (after correcting for
313 AMS lens transmission as above) had a slope of 1.06 for the entire SENEX study and 72% of
314 the data points were within the measurements' combined uncertainties of $\pm 45\%$ (Bahreini et al.,
315 2008). For the flight analyzed here, however, the same regression slope was 1.58, which is
316 slightly higher than the combined uncertainties. It is unclear why the two types of volume
317 measurements disagree more for this flight. This does not change the conclusions of this work
318 because this has been incorporated into the error in aerosol organic nitrate, which still show
319 positive enhancements in pRONO₂ for these plumes (see Figure 4 below). These complete
320 error estimates are also used in Figure 5 to clearly show the uncertainties in the yields. The
321 volume comparison is discussed further in the Supplemental Information and shown for the
322 plumes of interest in Fig. S1.

323
324 The C-ToF-AMS is a unit mass resolution (UMR) instrument and the mass spectral signals that
325 are characteristic of aerosol nitrate at m/z 30 and 46 (NO^+ and NO_2^+) often contain interferences
326 from organic species such as CH_2O^+ and CH_2O_2^+ , respectively. Here, the m/z 30 and 46 signals
327 have been corrected for these interferences by using correlated organic signals at m/z 29, 42,
328 43, and 45 that were derived from high-resolution AMS measurements during the NASA
329 SEAC⁴RS campaign that took place in the same regions of the SE US shortly after SENEX (see
330 Supplemental Information and Fig. S2). The corrections were applied to the individual flight
331 analyzed here from July 2. All of the corrections were well correlated with each other for the
332 SEAC⁴RS dataset and we used the organic peak at m/z 29 (from CHO^+) and the peak at m/z 45
333 (from CHO_2^+), respectively, since those corrections were from peaks closest (in m/z) to those
334 being corrected. Once corrected, the nitrate mass concentrations in the final data archive for
335 this flight were reduced by $0\text{-}0.24 \mu\text{g sm}^{-3}$, an average reduction of $0.11 \mu\text{g sm}^{-3}$ or 32% from
336 the initial nitrate mass concentrations. The organic interferences removed from the m/z 30 and
337 m/z 46 signals are linearly correlated with the total organic mass concentrations, corresponding
338 to an average 1.3% increase in the total organic mass.

339
340 The ratio of the corrected $\text{NO}_2^+/\text{NO}^+$ signals was then used to calculate the fraction of aerosol
341 nitrate that was organic (pRONO₂) or inorganic (ammonium nitrate) based on the method
342 described first in (Fry et al., 2013). Here we used an organic $\text{NO}_2^+/\text{NO}^+$ ratio that was equal to
343 the ammonium nitrate $\text{NO}_2^+/\text{NO}^+$ ratio from our calibrations divided by 2.8. This factor was
344 determined from multiple datasets (see discussion in Supplemental Information). The
345 ammonium nitrate $\text{NO}_2^+/\text{NO}^+$ ratio was obtained from the two calibrations on 30 June and 7 July

346 that bracketed the flight on 2 July, which is analyzed here. It was 0.514 and 0.488, respectively,
347 and for all of the data from both calibrations it averaged 0.490. Hence, the organic nitrate
348 $\text{NO}_2^+/\text{NO}^+$ ratio was estimated to be 0.175. This is the first time, to our knowledge, that UMR
349 measurements of aerosol nitrate have been corrected with HR correlations and used to
350 apportion the corrected nitrate into inorganic or organic nitrate species.

351
352 The time since emission of intercepted power plant plumes was estimated from the slope of a
353 plot of O_3 against NO_2 . For nighttime emitted NO_x plumes that consist primarily of NO (Peischl
354 et al., 2010), O_3 is negatively correlated with NO_2 due to the rapid reaction of NO with O_3 that
355 produces NO_2 in a 1:1 ratio:



358
359 Reaction R1 goes rapidly (NO pseudo first order loss rate coefficient of 0.03 s^{-1} at 60 ppb O_3) to
360 completion, so that all NO_x is present as NO_2 , as long as the plume NO does not exceed
361 background O_3 after initial mixing of the plume into background air. Subsequent oxidation of
362 NO_2 via reaction (R2) leads to an increasingly negative slope of O_3 vs NO_2 :



365
366 Equation (1) then gives plume age subsequent to the completion of (R1) in terms of the
367 observed slope, m , of O_3 vs NO_2 (Brown et al., 2006).

368
369
$$t_{\text{plume}} = \frac{\ln[1-S(m+1)]}{Sk_1\bar{\text{O}}_3} \quad (1)$$

370
371 Here S is a stoichiometric factor that is chosen for this analysis to be 1 based on agreement of
372 plume age with elapsed time in a box model run initialized with SENEX flight conditions (see
373 below); k_1 is the temperature dependent bimolecular rate constant for $\text{NO}_2 + \text{O}_3$ (R2) and $\bar{\text{O}}_3$ is
374 the average O_3 within the plume.

375
376 We calculate plume ages using both a stoichiometric factor of 1 (loss of NO_3 and N_2O_5
377 dominated by NO_3 reactions) and 2 (loss dominated by N_2O_5 reactions), although we note that
378 the chemical regime for $\text{NO}_3+\text{N}_2\text{O}_5$ loss may change over the lifetime of the plume, progressing
379 from 1 to 2 as the BVOC is consumed. We use $S=1$ values in the analysis that follows. Because
380 the more aged plumes are more likely to have S approach 2, this means that some of the older
381 plumes may have overestimated ages. Fig. S3 in the Supplemental Information shows the
382 plume age calculated by Eq. 1 using modeled NO_x , NO_y and O_3 concentrations for $S=1$ and
383 $S=2$, from nighttime simulations of plume evolution using an observationally constrained box
384 model. This confirms that for nighttime plumes, $S=1$ plume ages match modeled elapsed time
385 well. The model used for this calculation, and those used to assess peroxy radical lifetimes and
386 fates in Section 4.3, was the Dynamically Simple Model of Atmospheric Chemical Complexity
387 (DSMACC (Emmerson and Evans 2009)) containing the Master Chemical Mechanism v3.3.1
388 chemistry scheme (Jenkin et al., 2015). More details on the model approach are provided in the
389 SI.

390 **3 Nighttime flight selection**

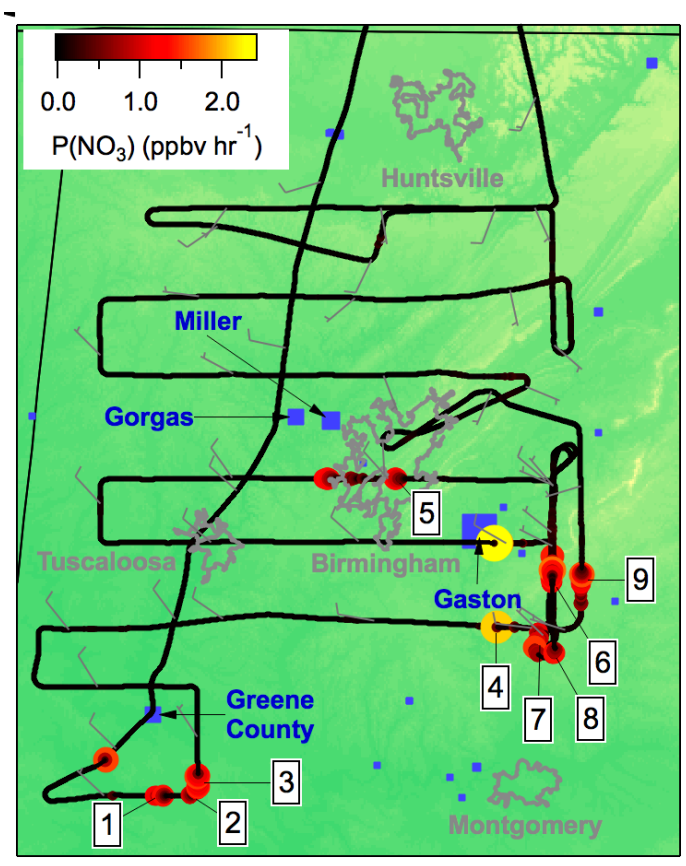
391 There were three nighttime flights (takeoffs on the evenings of 19 June, 2 July, and 3 July,
392 2013, local time) conducted during SENEX, of which one (2 July) surveyed regions surrounding
393 Birmingham, Alabama, including multiple urban and power plant plume transects. As described
394 in the introduction, these plume transects are the focus of the current analysis since they
395 correspond to injections of concentrated NO (and subsequently high $P(\text{NO}_3)$) into the regionally
396 widespread residual layer isoprene. The nighttime flight on 3 July, over Missouri, Tennessee
397 and Arkansas sampled air more heavily influenced by biomass burning than biogenic emissions.
398 The 19 June night flight sampled earlier in the evening, in the few hours immediately after
399 sunset, and sampled more diffuse urban plume transects that had less contrast with background
400 air. Therefore, this paper uses data exclusively from the 2 July flight, in which 9 transects of
401 well-defined NO_x plumes from power plants emitted during darkness can be analyzed to obtain
402 independent yields measurements.

403
404 A map of the 2 July flight track is shown in Fig. 1a. After takeoff at 8:08 pm local Central
405 Daylight Time on 2 July, 2013 (1:08 am UTC 3 July, 2016), the flight proceeded towards the
406 southwest until due west of Montgomery, AL, after which it conducted a series of east-west
407 running tracks while working successively north toward Birmingham, AL. Toward the east of
408 Birmingham, the aircraft executed overlapping north-south tracks at six elevations to sample the
409 E. C. Gaston power plant. During the course of the flight, concentrated NO_x plumes from the
410 Gaston, Gorgas, Miller and Greene City power plants were sampled. Around 1:30 and 2:30 AM
411 Central Daylight Time (5:30 and 6:30 am UTC), two transects of the Birmingham, AL urban
412 plume were measured prior to returning to the Smyrna, TN airport base.

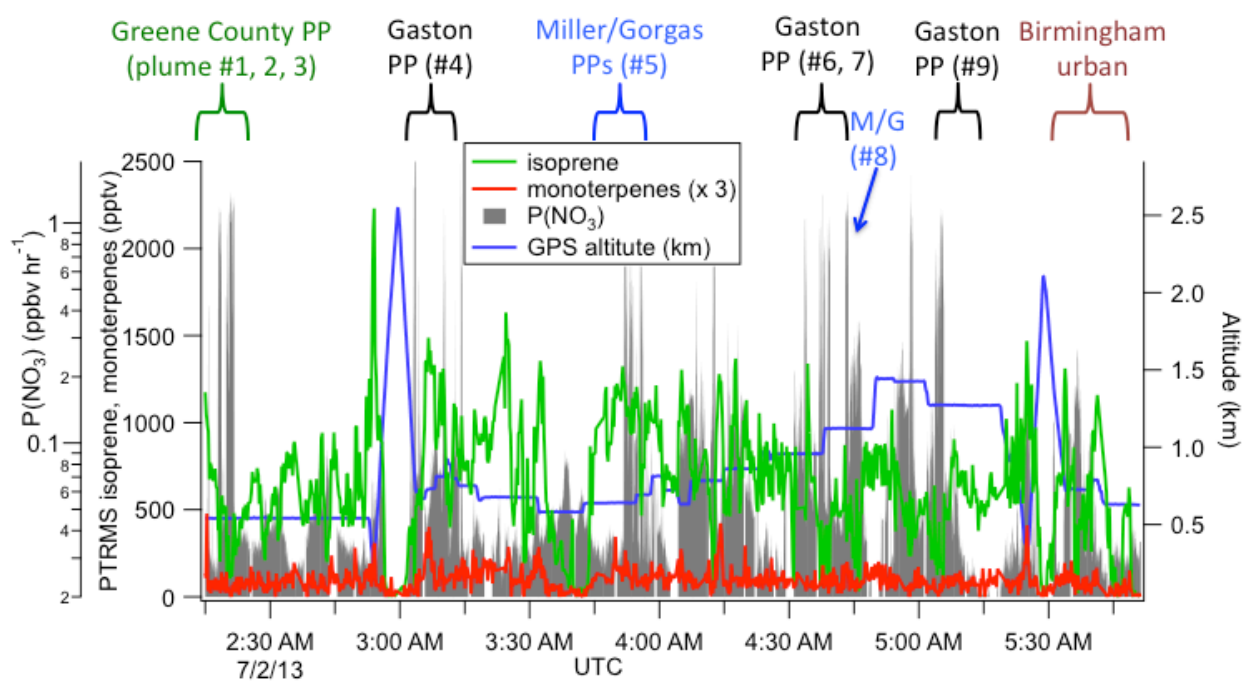
413
414 The flight track is shown colored by the nitrate radical production rate, $P(\text{NO}_3)$, to show the
415 points of urban and/or power plant plume influence:

$$416 \quad P(\text{NO}_3) = k_2(T) [\text{NO}_2][\text{O}_3] \quad (2)$$

417
418 Here, k_2 is again the temperature-dependent rate coefficient for reaction of $\text{NO}_2 + \text{O}_3$ (Atkinson
419 et al., 2004), and the square brackets indicate concentrations. Fig. 1b further illustrates the
420 selection of power plants plumes: sharp peaks in $P(\text{NO}_3)$ are indicative of power plant plume
421 transects, during which isoprene mixing ratios also are observed to drop from the typical
422 regional residual layer background values of ~ 1 ppb, indicative of loss by NO_3 oxidation (an
423 individual transect is shown in more detail below in Fig. 2). Also shown in Fig. 1b are measured
424 concentrations of isoprene and monoterpenes throughout the flight, showing substantial residual
425 layer isoprene and supporting the assumption that effectively all NO_3 reactivity is via isoprene
426 (see calculation in next section). Residual layer concentrations of other VOCs that could
427 produce SOA (e.g., aromatics) are always below 100 pptv, and their reaction rates with NO_3 are
428 slow. Edwards *et al.* (Edwards et al., 2017) have shown that NO_3 and isoprene mixing ratios for
429 this and other SENEX night flights exhibit a strong and characteristic anticorrelation that is
430 consistent with nighttime residual layer oxidation chemistry.
431
432



433 1a
 434 1b



435
 436
 437
 438

Figure 1a. Map of northern Alabama, showing the location of the flight track of the 2 July 2013 night flight used in the present analysis, with plume numbers labeled and wind direction shown. Although the wind direction changed throughout the night, these measurements enable us to

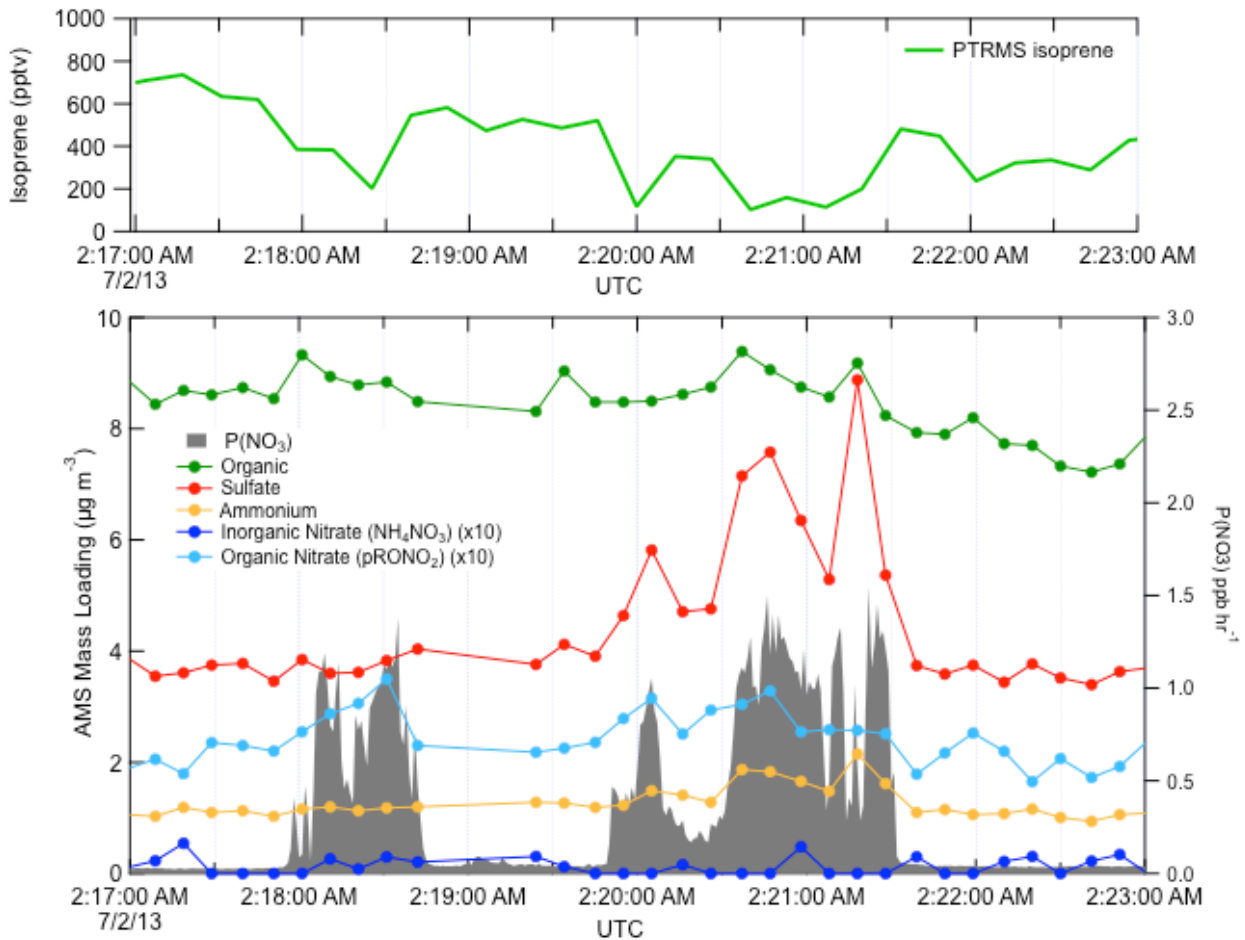
439 attribute each plume to a power plant source (see labels in Figure 1b and Table 2). Color scale
440 shows $P(\text{NO}_3)$ based on aircraft-measured $[\text{NO}_2]$ and $[\text{O}_3]$, while power plants discussed in the
441 text are indicated in blue squares with marker size scaled to annual NO_x emissions for 2013
442 (scale not shown). Isoprene emissions are widespread in the region (Edwards et al., 2017).
443 **Figure 1b** shows time series data from the same flight, with plume origins and numbers labeled,
444 showing aircraft-measured isoprene and monoterpene concentrations, altitude, and $P(\text{NO}_3)$
445 determined according to Eq. 2 (log scale), showing that the isoprene was uniformly distributed
446 (mixing ratios often in excess of 1 ppbv), while the more reactive monoterpenes were present at
447 mixing ratios below 100 ppt except at the lowest few hundred meters above ground in the
448 vertical profiles (not used in the present analysis). Figure 1b also shows that sharp peaks in
449 nitrate radical production rate occur both at the lowest points of these vertical profiles, when the
450 aircraft approached the surface, but also frequently during periods of level flight in the residual
451 layer, which correspond to the power plant plume transects analyzed in this paper.

452 **4 Results**

453 **4.1 Selection of plumes**

454 Figure 2 shows a subset of the July 2 flight time series data, illustrating three NO_x plumes used
455 for analysis. The large NO_3 source and isoprene loss was accompanied by an increase in
456 organic nitrate aerosol mass, which we attribute to the $\text{NO}_3 + \text{isoprene}$ reaction based on prior
457 arguments. We observed each plume as a rapid and brief perturbation to background
458 conditions, of order 10 – 50 sec., or 1 – 5 km in spatial scale. Each plume's perturbed
459 conditions can correspond to different plume ages, depending on how far downwind of the
460 power plant the plume transect occurred.

461



462

463

464

465

466

467

468

469

Figure 2. Three representative plume transect observations from the 2 July 2013 flight (plumes are identified by the peaks in $P(\text{NO}_3)$, listed in Table 1 at times 02:18, 02:20, and 02:21 UTC). Note the difference in sulfate enhancement in the three plumes, which is largest in the third plume, and is accompanied by increases in ammonium. In all three cases, the isoprene concentration drops in the plumes, accompanied by a clear increase in organic nitrate, no changes in the inorganic nitrate, and a modest changes in organic aerosol mass concentrations.

470

471

472

473

474

475

476

477

478

479

480

Candidate plumes were initially identified by scanning the time series flight data for any period where the production rate of nitrate radical ($P(\text{NO}_3)$) rose above 0.5 ppbv hr^{-1} . This threshold was chosen to be above background noise and large enough to isolate only true plumes (see Fig. 1a). The value is thus subjectively chosen, but was consistently applied across the dataset. For each such period, a first screening removed any of these candidate plumes that occurred during missed approaches or other periods where radar altitude above ground level (AGL) was changing, because in the stratified nighttime boundary layer structure, variations in altitude may result in sampling different air-masses, rendering the adjacent out of plume background not necessarily comparable to in-plume conditions. A second criterion for rejection of a plume was missing isoprene or AMS data during brief plume intercepts. No selected plumes on July 2 showed enhanced acetonitrile or refractory black carbon, indicating no significant biomass

481 burning influence. Finally, two plumes downwind of the Gaston power plant (at 03:10 and
482 03:14) were removed from the present analysis, because (03:10) the background isoprene was
483 changing rapidly, preventing a good baseline measurement, and (03:14) there was no observed
484 decrease in isoprene concentration in-plume (as well as no increase in nitrate aerosol). The
485 03:14 plume was apparently too recently emitted to have undergone significant nighttime
486 reaction; its O_3/NO_2 slope was unity to within the combined measurement error of O_3 and NO_2
487 (Eq. 1). After this filtering, there are 9 individual plume observations for determination of NO_3 +
488 isoprene SOA yields (see Table 1). The rapid increases in $P(NO_3)$ appeared simultaneously with
489 significant decreases in isoprene and increases in aerosol nitrate. The aerosol and isoprene
490 measurements (taken at data acquisition rates < 1 Hz) were not exactly coincident in time which
491 leads to some uncertainty in the yield analysis below.

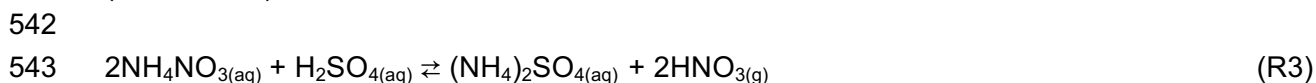
492
493 Derivation of SOA yields from observed changes in isoprene and aerosol mass in plumes
494 depends on two conditions, and has several caveats that will be discussed in the text that
495 follows (see Table 3 below for a summary of these caveats). The two conditions are: (1) that the
496 majority of VOC mass consumed by NO_3 in plumes is isoprene (rather than monoterpenes or
497 other VOC), and then either or both (2a) that the change in aerosol organic mass concentration
498 during these plumes is due to NO_3 + isoprene reactions, and/or (2b) that the change in aerosol
499 nitrate mass concentration is due to NO_3 + isoprene reactions. There are separate
500 considerations for each of these conditions.

501
502 For the first condition, we note that the isoprene to monoterpenes ratio just outside each plume
503 transect was always high (a factor of 10 to 70, on average 26). With the 298 K NO_3 rate
504 constants of $\sim 5 \times 10^{-12} \text{ cm}^3 \text{ molec}^{-1} \text{ s}^{-1}$ for monoterpenes and $6.5 \times 10^{-13} \text{ cm}^3 \text{ molec}^{-1} \text{ s}^{-1}$ for
505 isoprene (Calvert et al., 2000), isoprene (~ 2 ppb) will always react faster with nitrate than
506 monoterpenes (~ 0.04 ppbv). At these relative concentrations, even if all of the monoterpene is
507 oxidized, the production rate of oxidation products will be much larger for isoprene. Contribution
508 to aerosol by N_2O_5 uptake is also not important in these plumes. Edwards et al. (Edwards et al.,
509 2017) calculated the sum of NO_3 and N_2O_5 loss throughout this flight and showed that it is
510 consistently NO_3 +BVOC dominated (Fig. S4 of that paper). As isoprene depletes, N_2O_5 uptake
511 will increasingly contribute to NO_3 loss, but as shown below, we are able to rule out a
512 substantial source of inorganic nitrate for most plumes. We also know that despite increased
513 OH production in-plume, the isoprene loss is still overwhelmingly dominated by NO_3 (Fig. S5 in
514 Edwards, et al. (Edwards et al., 2017)) .

515
516 The second condition requires that we can find an aerosol signal that is attributable exclusively
517 to NO_3 + isoprene reaction products, whether it be organic aerosol (OA) or organic nitrate
518 aerosol ($pRONO_2$) mass loading, or both. We note that the ratio of in-plume aerosol organic
519 mass increase to $pRONO_2$ mass increase is noisy (see discussion below at Fig. 6), but indicates
520 an average in-plume ΔOA to $\Delta pRONO_2$ ratio of about 5. The large variability is primarily due to
521 the fact that the variability in organic aerosol mass between successive 10-second data points
522 for the entire flight is quite large (of order $0.75 \mu\text{g m}^{-3}$) and comparable to many of the individual
523 plume ΔOA increases, far exceeding the expected organonitrate driven increases in OA, which
524 are roughly twice the $pRONO_2$ mass increases. It is also possible that in these plumes, where

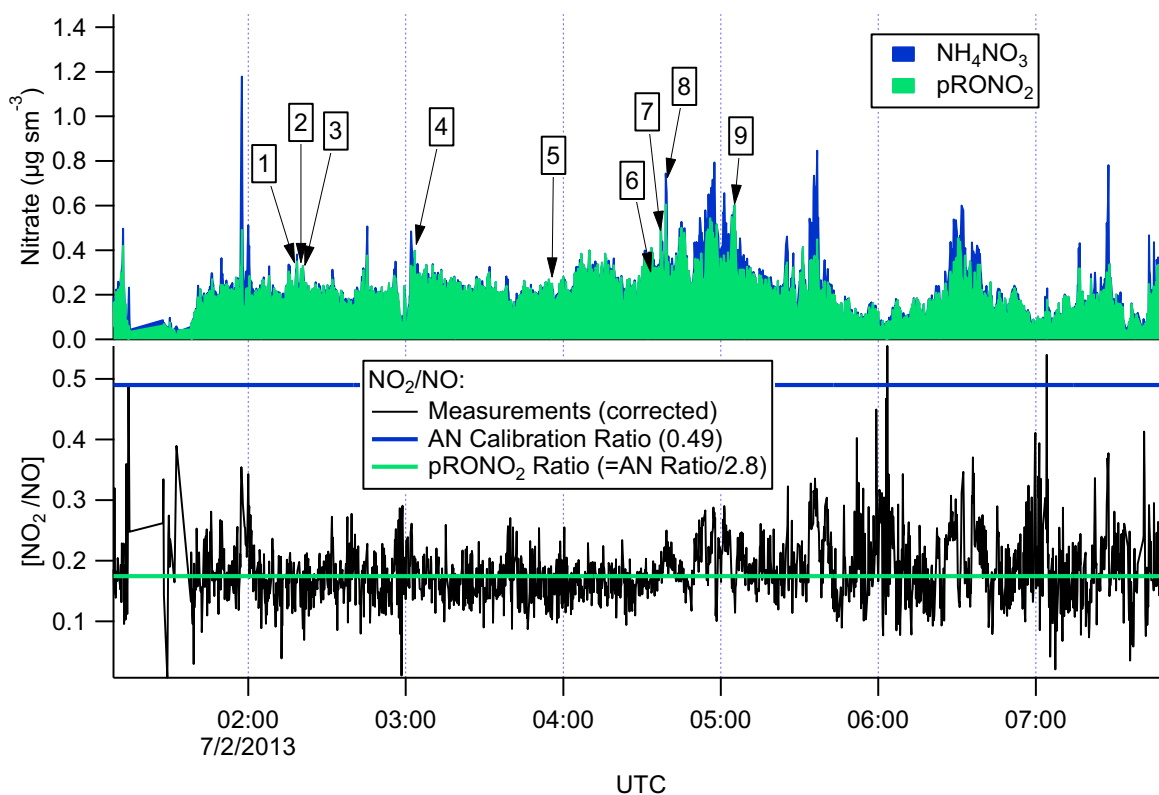
525 total aerosol mass is elevated, semivolatile organic compounds may re-partition to the aerosol
526 phase, contributing a non-pRONO₂ driven variability in ΔOA. For example, if some gas phase
527 IEPOX is present in the residual layer, it may be taken up into the highly acidic aerosol from the
528 power plants. Alternatively, very polar gas-phase compounds could partition further into the
529 higher liquid water associated with the sulfate in the plume. Therefore, in-plume organic aerosol
530 increases cannot be attributed clearly to NO₃ + isoprene SOA production, so we do not use
531 them in the SOA yield calculations.

532
533 This leaves consideration 2b, whether all increase in nitrate mass is due to NO₃ + isoprene
534 reactions. Here we must evaluate the possibility of inorganic nitrate aerosol production in these
535 high-NO_x plumes. Fine-mode aerosol inorganic nitrate can be formed by the (reversible)
536 dissolution of HNO_{3(g)} into aqueous aerosol. In dry aerosol samples, inorganic nitrate is typically
537 in the form of ammonium nitrate (NH₄NO₃), when excess ammonium is available after
538 neutralization of sulfate as (NH₄)₂SO₄ and NH₄(HSO₄). Because of the greater stability of
539 ammonium sulfate salt relative to ammonium nitrate, in high-sulfate plumes with limited
540 ammonium, inorganic nitrate aerosol will typically evaporate as HNO_{3(g)} (Guo et al., 2015)
541 (reaction R3):



545 Inorganic nitrate can also form when crustal dust (e.g. CaCO₃) or seasalt (NaCl) are available.
546 Uptake of HNO₃ is rendered favorable by the higher stability of nitrate mineral salts, evaporating
547 CO₂ or HCl. Inorganic nitrate can also be produced by the heterogeneous uptake of N₂O₅ onto
548 aqueous aerosol; Edwards et al. (2017) demonstrated that this process is negligible relative to
549 NO₃ + BVOC for the July 2 SENEX night flight considered here.

550
551 There are several lines of evidence that the observed nitrate aerosol is organic and not
552 inorganic. First, examination of the NO₂⁺/NO⁺ (interference-corrected *m/z* 46:*m/z* 30) ratio
553 measured by the aircraft AMS (Fig. 3) shows a ratio throughout the July 2 flight, including the
554 selected plumes, that is substantially lower than that from the bracketing ammonium nitrate
555 calibrations. This lower AMS measured NO₂⁺/NO⁺ ratio has been observed for organic nitrates
556 (Farmer et al., 2010), and some mineral nitrates (e.g. Ca(NO₃)₂ and NaNO₃, (Hayes et al.,
557 2013)), which are not important in this case because aerosol was dominantly submicron. As
558 described above, we can separate the observed AMS nitrate signal into pRONO₂ and inorganic
559 nitrate contributions. These mass loadings are also shown in Fig. 3, indicating dominance of
560 pRONO₂ throughout the flight.



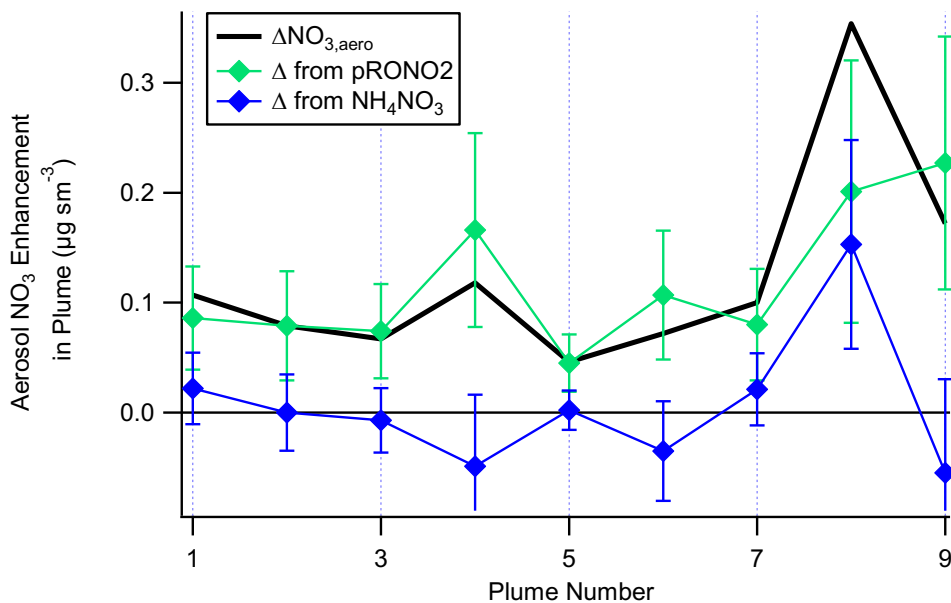
562
 563 **Figure 3.** For the flight under consideration, the estimated relative contributions of ammonium
 564 and organic nitrate to the total corrected nitrate signal (top panel) was calculated from the ratios
 565 of the corrected peaks at m/z 30 and 46 (lower panel). Each of the plumes is identified here by
 566 plume number. The ratios of $\text{NO}_2^+/\text{NO}^+$ (black data in the lower panel) from the corrected peaks
 567 at m/z 46 and 30, respectively, are compared to the ratios expected for ammonium nitrate (AN
 568 Calibration Ratio, blue horizontal line at 0.49) or organic nitrate (pRONO₂ Ratio, green
 569 horizontal line at 0.175 which is estimated from the AN calibration ratio using multiple data sets
 570 (see discussion in Supplemental Information). The measured ratio for most of the flight is more
 571 characteristic of organic nitrate than ammonium nitrate.

572
 573 We can also employ the comparison of other AMS-measured aerosol components during the
 574 individual plumes to assess the possibility of an inorganic nitrate contribution to total measured
 575 nitrate. Fig. S5a shows that the in-plume increases in sulfate are correlated with increases in
 576 ammonium with an R^2 of 0.4. The observed slope of 5.4 is characteristic of primarily $(\text{NH}_4)\text{HSO}_4$,
 577 which indicates that the sulfate mass is not fully neutralized by ammonium. We note, however,
 578 that if the largest observed aerosol nitrate increase is due solely to ammonium nitrate, the
 579 ammonium increase would be only $0.11 \mu\text{g m}^{-3}$, which would be difficult to discern from the NH_4
 580 variability of order $0.11 \mu\text{g m}^{-3}$. However, the slope is consistent with incomplete neutralization
 581 of the sulfate by ammonium, which would make $\text{HNO}_{3(g)}$ the more thermodynamically favorable
 582 form of inorganic nitrate. The ion balance for the ammonium nitrate calibration particles and the
 583 plume enhancements are shown in Fig. S5b. Complete neutralization of the calibration aerosols
 584 is nearly always within the gray 10% uncertainty band for the relative ionization efficiency of

585 ammonium (Bahreini et al., 2009). In contrast, many of the plume enhancements are near the
 586 1:2 line (as primarily ammonium bisulfate) within the combined 10% ammonium and 15%
 587 sulfate uncertainty error bars or without ammonium (sulfuric acid). Thus, NH_4NO_3 is unlikely to
 588 be stable in the aerosol phase under the conditions of these plumes, consistent with the AMS
 589 observations.

590

591 A plot of the calculated plume enhancements from the derived apportionment into organic
 592 (pRONO_2) and inorganic (ammonium) nitrate is shown in Fig. 4. The increases in aerosol nitrate
 593 for nearly all of the plumes appear to be mostly due to enhancements in pRONO_2 . Based on
 594 these considerations, we conclude that in-plume pRONO_2 mass increases are a consequence
 595 (and thus a robust measure) of organic nitrate aerosol produced from $\text{NO}_3 + \text{isoprene}$. Since
 596 each isoprene molecule condensing will have one nitrate group, the ratio of these increases to
 597 isoprene loss is a direct measure of the molar organic aerosol yield from NO_3 -isoprene
 598 oxidation.



599

600

601 **Figure 4.** The contribution of each species to the nitrate enhancements in each of the plumes,
 602 showing that the enhancements in most of the plumes are mainly due to enhancements in
 603 organic nitrate, with the exception of Plume 8 which had enhancements in both organic and
 604 ammonium nitrate. Error bars are estimated from the measurement variability, the UMR
 605 corrections to the nitrate signals, apportionment between organic and inorganic nitrate, and the
 606 total nitrate uncertainty (see Supplemental Information).

607

608 Table 1 shows the selected plumes to be used for yield analysis. Wherever possible, multiple
 609 points have been averaged for in-plume and background isoprene and nitrate aerosol
 610 concentrations; in each case the number of points used is indicated and the corresponding
 611 standard deviations are reported. In two cases (2:20 and 3:03 plumes), the plumes were so
 612 narrow that only a single point was measured in-plume at the 10 s time resolution of the PTR-

613 MS and AMS; for these “single-point” plumes it is not possible to calculate error bars. Error bars
614 were determined using the standard deviations calculated for in-plume and background
615 isoprene and nitrate aerosol concentrations, accounting also for the additional uncertainty in the
616 AMS measurement described in the caption to Figure 4, and propagated through the yield
617 formula detailed in the following section.
618

619 **Table 1.** List of plumes used in this NO₃ + isoprene SOA yield analysis. For each plume, the
620 delta-values listed indicate the difference between in-plume and outside-plume background in
621 average observed concentration, and the standard deviations (SD) are the propagated error
622 from this subtraction. (For ΔNO₃ from pRONO₂, the standard deviations also include error
623 propagated from the uncertainties in the nitrate apportionment and aerosol volume, as
624 described in the caption for Figure 4) After each plume number, the numbers of points averaged
625 for isoprene (10 s resolution) and AMS (10 s resolution), respectively, are listed. Because the
626 isoprene data were reported at a lower frequency, these numbers are typically lower to cover
627 the same period of time. Plume numbers annotated with * indicate brief plumes for which only
628 single-point measurements of in-plume aerosol composition were possible. Additional AMS and
629 auxiliary data from each plume is included in the Supplemental Information, Table S3.

plume number [#isop/#AMS]	7/2/13 plume time (UTC)	P(NO ₃) (ppbv hr ⁻¹)	ΔISOP (ppt) [± SD]	ΔNO _{3,aero} (μg m ⁻³) [± SD]	ΔNO ₃ from pRONO ₂ (μg m ⁻³) [± SD]	ΔNO ₃ from NH ₄ NO ₃ (μg m ⁻³) [± SD]
Typical variability (μg m ⁻³):				0.05	0.05	0.05
1 [2/3]	2:18	0.9	-335 [128]	0.107 [0.039]	0.086 [0.047]	0.022 [0.012]
2 [*]	2:20	0.8	-404	0.079	0.079	0
3 [4/5]	2:21	1.2	-228 [121]	0.067 [0.039]	0.074 [0.043]	-0.007 [0.027]
4 [*]	3:03	1.4	-453	0.118	0.166	-0.049
5** [3/4]	3:55	1.0	-255 [251]	0.046 [0.019]	0.045 [0.026]	0.002 [0.015]
6 [2/2]	4:34	0.6	-713 [219]	0.072 [0.031]	0.107 [0.059]	-0.035 [0.029]
7 [5/6]	4:37	0.8	-298 [197]	0.100 [0.082]	0.080 [0.051]	0.021 [0.034]
8*** [2/3]	4:39	0.9	-443 [75]	0.354 [0.058]	0.201 [0.12]	0.153 [0.057]
9 [7/8]	5:04	0.6	-293 [131]	0.172 [0.048]	0.227 [0.115]	-0.055 [0.042]

630 **Plume 5 has the smallest ΔNO_{3,aero} and may be affected by background pRONO₂ variability.

631 ***Plume 8 has a measurable increase in inorganic nitrate as well as organic.

632 4.2 SOA yield analysis

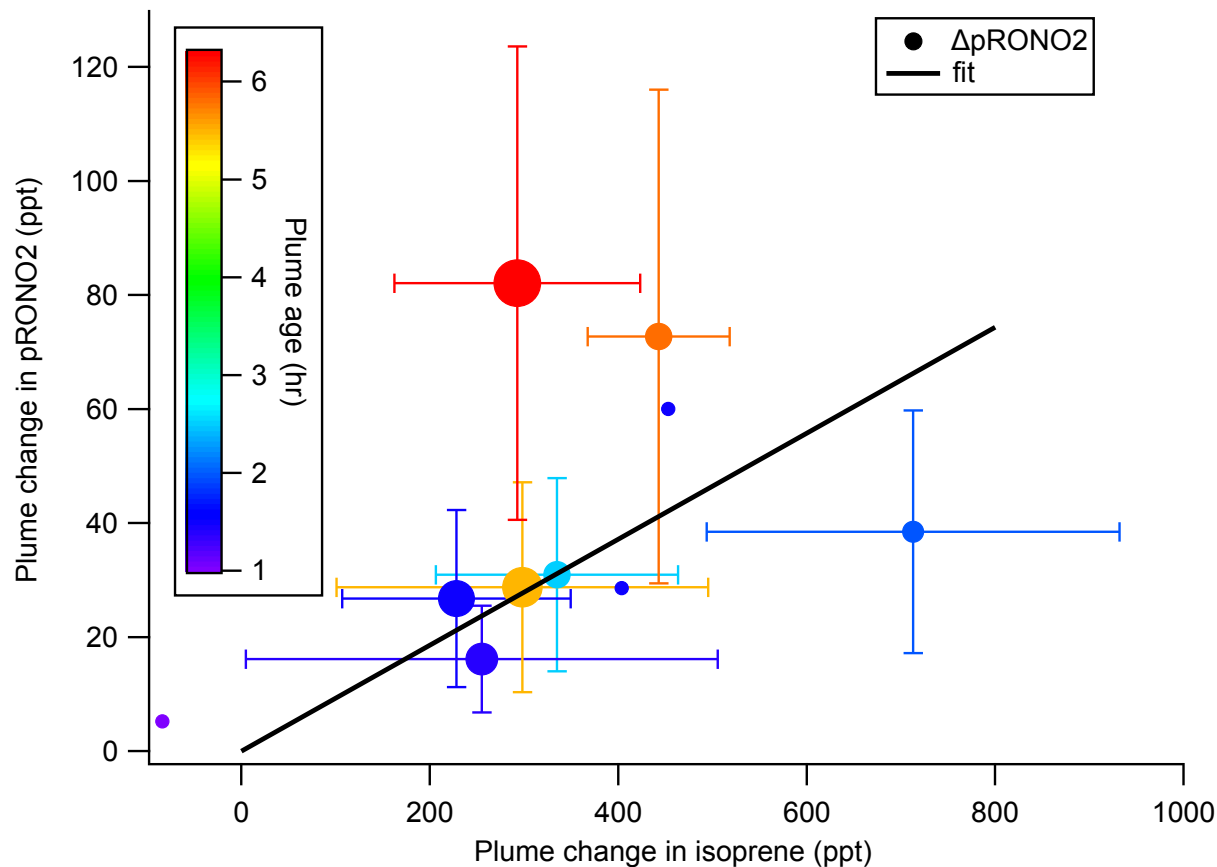
633 A **molar** SOA yield refers to the number of molecules of aerosol organic nitrate produced per
634 molecule of isoprene consumed. In order to determine molar SOA yields from the data
635 presented in Table 1, we convert the aerosol organic nitrate mass loading differences to mixing
636 ratio differences (ppt) using the NO₃ molecular weight of 62 g mol⁻¹ (the AMS organic nitrate

637 mass is the mass only of the $-\text{ONO}_2$ portion of the organonitrate aerosol). At standard
 638 conditions of 273 K and 1 atm (all aerosol data are reported with this STP definition), 1000 ppt
 639 $\text{NO}_3 = 2.77 \mu\text{g m}^{-3}$, so each $\Delta M_{p\text{RONO}_2}$ is multiplied by $361 \text{ ppt } (\mu\text{g m}^{-3})^{-1}$ to determine this molar
 640 yield:

$$642 Y_{\text{SOA,molar}} = \frac{(p\text{RONO}_2_{\text{plume}} \pm SD_{p\text{RONO}_2_{\text{plume}}}) - (p\text{RONO}_2_{\text{bkg}} \pm SD_{p\text{RONO}_2_{\text{bkg}}})}{-[(isop_{\text{plume}} \pm SD_{isop_{\text{plume}}}) - (isop_{\text{bkg}} \pm SD_{isop_{\text{bkg}}})]} \times \frac{361 \text{ ppt } \text{NO}_3}{\mu\text{g m}^{-3}} \quad (3)$$

643
 644 The SOA molar yields resulting from this calculation are shown in Table 2, spanning a range of
 645 5-28%, with uncertainties indicated based on the SDs in measured AMS and isoprene
 646 concentrations. In addition to this uncertainty based on measurement precision and ambient
 647 variability, there is an uncertainty of 50% in the AMS derived-organic nitrate mass loadings (see
 648 SI) and 25% in the PTR-MS isoprene concentrations (Warneke et al., 2016). The average molar
 649 $p\text{RONO}_2$ yield across all plumes, with each point weighed by the inverse of its standard
 650 deviation and assuming $SD = 0.1$ for single point plumes, is 9%. (As noted below, the yield
 651 appears to increase with plume age, so this average obscures that trend.) An alternate
 652 graphical analysis of molar SOA yield from all nine plumes plus one 'null' plume (03:14, in which
 653 no isoprene had yet reacted and thus not included in Tables 1 and 2) obtains the same average
 654 molar yield of 9% (Fig. 5). Here, the molar yield is the slope of a plot of plume change in
 655 $p\text{RONO}_2$ vs plume change in isoprene. The slope is determined by a linear fit with points
 656 weighted by the square root of the number of AMS data points used to determine in-plume
 657 $p\text{RONO}_2$ in each case. We have not corrected the calculated yields for the possibility of NO_3
 658 heterogeneous uptake, which could add a nitrate functionality to existing aerosol. Such a
 659 process could be rapid if the uptake coefficient for NO_3 were 0.1, a value characteristics of
 660 unsaturated substrates (Ng et al., 2017), but would not contribute measurably at more
 661 conventional NO_3 uptake coefficients of 0.001 (Brown and Stutz 2012).

662
 663

665
666

667 **Figure 5.** SOA molar yield can be determined as the slope of $\Delta p\text{RONO}_2$ vs. Δ isoprene, both in
 668 mixing ratio units. The linear fit is weighted by square root of number of points used to
 669 determine each in-plume $p\text{RONO}_2$, with intercept held at zero. The slope coefficient \pm one
 670 standard deviation is 0.0930 ± 0.0011 . Points are colored by plume age, and size scaled by
 671 square root of number of points (the point weight used in linear fit). This plot and fit includes the
 672 nine plumes listed in Tables 1 and 2, as well as the 03:14 “unreacted” plume (at Δ isoprene = -
 673 84 ppt). Error bars on isoprene are the propagated standard deviations of the (in plume - out
 674 plume) differences, for plumes in which multi-point averages were possible. Error bars on
 675 $p\text{RONO}_2$ are the same as in Figure 4. The points without error bars are single-point plumes.

676

677 To estimate SOA **mass** yields, we need to make some assumption about the mass of the
 678 organic molecules containing the nitrate groups that lead to the observed nitrate aerosol mass
 679 increase. The observed changes in organic aerosol are too variable to be simply interpreted as
 680 the organic portion of the aerosol organic nitrate molecules. We conservatively assume the
 681 organic mass to be approximately double the nitrate mass (62 g mol^{-1}), based on an “average”
 682 molecular structure of an isoprene nitrate with 3 additional oxygens: e.g. a tri-hydroxynitrate
 683 (with organic portion of formula $\text{C}_5\text{H}_{11}\text{O}_3$, 119 g mol^{-1}), consistent with 2nd-generation oxidation
 684 product structures suggested in Schwantes, et al. (Schwantes et al., 2015). Based on this
 685 assumed organic to nitrate ratio, all plumes’ expected organic mass increases would be less

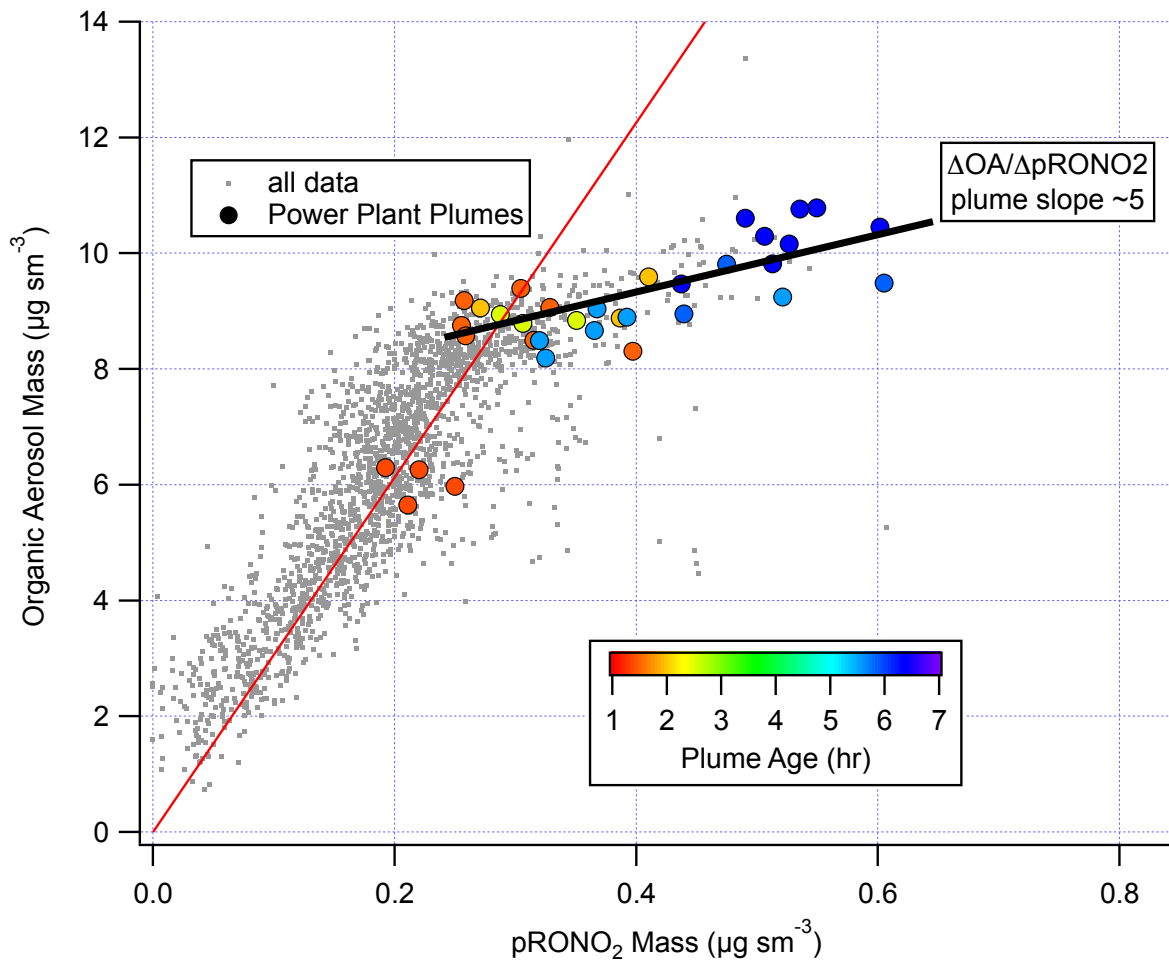
686 than the typical variability in organic of $0.75 \mu\text{g m}^{-3}$. This assumed structure is consistent with
 687 oxidation of both double bonds, which appears to be necessary for substantial condensation of
 688 isoprene products, and which structures would have calculated vapor pressures sufficiently low
 689 to partition to the aerosol phase (Rollins et al., 2009). Another possible route to low vapor
 690 pressure products is intramolecular H rearrangement reactions, discussed below in Section 4.3,
 691 which would not require oxidant reactions at both double bonds. In the case of oxidant reactions
 692 at both double bonds, it is difficult to understand how the second double bond would be oxidized
 693 unless by another nitrate radical, which would halve these assumed organic to nitrate ratios
 694 (assuming the nitrate is retained in the molecules). On the other hand, any organic nitrate
 695 aerosol may lose NO_3 moieties, increasing the organic to nitrate ratio. Given these uncertainties
 696 in both directions, we use the assumed “average” structure above to guess an associated
 697 organic mass of double the nitrate mass. Thus, to estimate SOA mass yield, we multiply the
 698 increase in organic nitrate aerosol mass concentration by three (i.e., $2 \times \Delta M_{p\text{RONO}_2} + \Delta M_{p\text{RONO}_2}$),
 699 and divide by the observed decrease in isoprene, converted to $\mu\text{g m}^{-3}$ by multiplying by 329 ppt
 700 ($\mu\text{g m}^{-3}$)⁻¹, the conversion factor based on isoprene’s molecular weight of 68.12 g mol^{-1} .

$$702 \quad Y_{\text{SOA, mass}} = \frac{(p\text{RONO}_2_{\text{plume}} \pm SD_{p\text{RONO}_2_{\text{plume}}}) - (p\text{RONO}_2_{\text{bkg}} \pm SD_{p\text{RONO}_2_{\text{bkg}}})}{-[(isop_{\text{plume}} \pm SD_{isop_{\text{plume}}}) - (isop_{\text{bkg}} \pm SD_{isop_{\text{bkg}}})]} \times 3 \times \frac{329 \text{ ppt}}{\mu\text{g m}^{-3}} \quad (4)$$

703
 704 Note that the SOA mass yield reported here is based on the (assumed) mass of organic aerosol
 705 plus the (organo)nitrate aerosol formed in each plume. If instead the yield were calculated using
 706 only the assumed increase in **organic** mass (i.e., $2 \times \Delta M_{p\text{RONO}_2}$ instead of $3 \times \Delta M_{p\text{RONO}_2}$), which
 707 would be consistent with the method used in Rollins, et al. (Rollins et al., 2009) and Brown et al.
 708 (Brown et al., 2009), the mass yields would be 2/3 the values reported here. However, since
 709 SOA mass yield is typically defined based on the total increase in aerosol mass, we use the
 710 definition with the sum of the organic and nitrate mass here.

711
 712 We note also that correlation of in-plume increases in OA with $p\text{RONO}_2$ (Fig. 6) point to a
 713 substantially larger 5:1 organic-to-nitrate ratio; if this were interpreted as indicating that the
 714 average molecular formula of the condensing organic nitrate has 5 times the organic mass as
 715 nitrate, this would increase the SOA mass yields reported here. However, due to the
 716 aforementioned possibility of additional sources of co-condensing organic aerosol, which led us
 717 to avoid using ΔOA in determining SOA yields, we do not consider this to be a direct indication
 718 of the molecular formula of the condensing organic nitrate. Including OA in the SOA yield
 719 determination, based on this 5:1 slope rather than the assumed 2:1 OA: $p\text{RONO}_2$, would give 2.5
 720 times larger SOA mass yields than reported here.

721



722

723 **Figure 6.** Correlation of organic aerosol mass concentration with pRONO₂ mass concentration
 724 for the full 2 July flight (grey points and red fit line, fitted slope and thus average OA/pRONO₂
 725 mass ratio of ~ 30) and for the points during the selected plumes (colored points, colored by
 726 plume age, average OA/pRONO₂ mass ratio of ~ 5).

727

728

729 **Table 2.** SOA Yields for each plume observation, estimated plume age, and likely origin. See
 730 text for description of uncertainty estimates. For the mass yields, the calculated SOA mass
 731 increase includes both the organic and (organo)nitrate aerosol mass; the measurements for OA
 732 increases shown in Figure 6 do not include the nitrate mass.

plume number	plume time (UTC)	SOA molar yield (fraction) [± SD]	SOA mass yield (fraction) [± SD]	plume age from O ₃ / NO ₂ clock assuming S=1 (hours)	Likely NO _x origin & altitude (m)
1	7/2/13 2:18	0.09 [0.06]	0.25 [0.17]	2.5	Greene County @ 540 m
2	7/2/13 2:20	0.07	0.21	1.5	<i>ibid</i>
3	7/2/13 2:21	0.12 [0.10]	0.32 [0.25]	1.5	<i>ibid</i>
4	7/2/13 3:03	0.13	0.36	1.5	Gaston @ 720 m
5	7/2/13 3:55	0.06 [0.07]	0.17 [0.20]	1.4	Miller / Gorgas @ 690 m
6	7/2/13 4:34	0.05 [0.03]	0.15 [0.09]	2	<i>ibid</i>
7	7/2/13 4:37	0.10 [0.09]	0.26 [0.24]	5.5	<i>ibid</i>
8	7/2/13 4:39	0.16 [0.10]	0.45 [0.28]	5.8	Miller / Gorgas @ 1120 m
9	7/2/13 5:04	0.28 [0.19]	0.77 [0.52]	6.3	Gaston @ 1280 m

733
734

735 **Table 3.** Several caveats to the present SOA yields analysis are listed below, alongside the
 736 expected direction each would adjust the estimated yields. Because we do not know whether or
 737 how much each process may have occurred in the studied plumes, we cannot quantitatively
 738 assess the resulting uncertainties, so we simply list them here. See text above for more detailed
 739 discussion.

Process	Effect on determined SOA yield
Organic nitrate aerosol loses NO ₃ functional group	Larger, because the non-nitrate OA would not be counted in this analysis
Both double bonds in isoprene are oxidized by NO ₃ : two nitrates per condensing molecule	Smaller, because the assumed organic to nitrate mass ratio assumes one nitrate per molecule
NO ₃ oxidizes daytime isoprene oxidation products (e.g. ISOPOOH) to make new aerosol	Smaller, because this would produce organic nitrate aerosol without corresponding decrease in isoprene, so that some of existing SOA production is mis-attributed to isoprene + NO ₃
Assumed organic to nitrate mass ratio is incorrect	Unknown direction of effect, depends on whether assumed ratio is high or low
Daytime-produced IEPOX uptake onto acidic particles	No effect (only changes ΔOA, not nitrate)
Suppression of O ₃ + monoterpene or O ₃ + isoprene SOA in plumes	No effect (only changes ΔOA, not nitrate)

740
 741 Finally, the large range in observed yields can be interpreted by examining the relationship to
 742 estimated plume age. Using the slope of O₃ to NO₂ (Eq. 1) to estimate plume age as described
 743 above, a weak positive correlation is observed (Table 2, Fig. S4), suggesting that as the plume
 744 ages, later-generation chemistry results in greater partitioning to the condensed phase of NO₃ +
 745 isoprene organonitrate aerosol products. This is consistent with the observation by Rollins et al.
 746 (Rollins et al., 2009) that 2nd-generation oxidation produced substantially higher SOA yields
 747 than the oxidation of the first double bond alone, but we note that these mass yields (averaging
 748 27%, would be 18% using the organic mass only) are higher than even the largest yield found in
 749 that chamber study (14%, used organic mass only).

750
 751 We observe increasing SOA yield, from a molar yield of around 10% at 1.5 hours up to 30% at 6
 752 hours of aging. The lowest yields observed are found in the most recently emitted plumes,
 753 suggesting the interpretation of the higher yields as a consequence of longer aging timescales
 754 in the atmosphere.

755 **4.3 Mechanistic considerations**

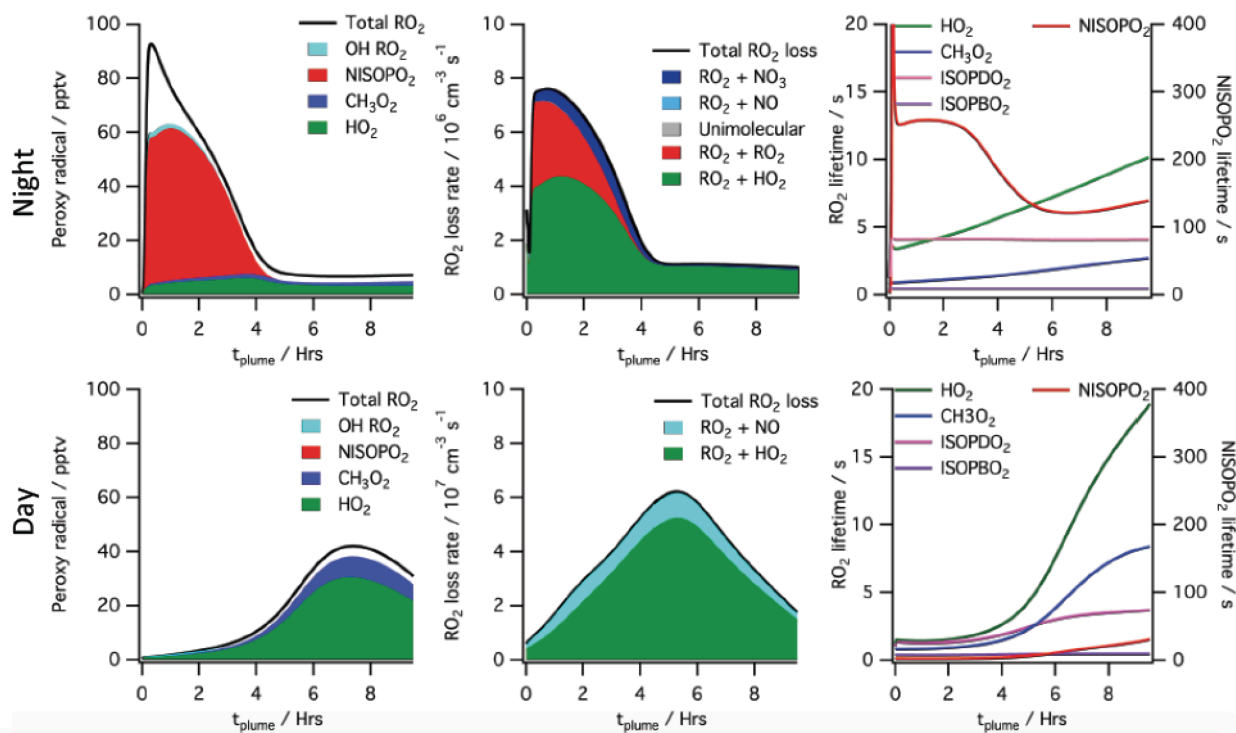
756
 757 These larger SOA mass yields from field determinations (average 27%) relative to chamber
 758 work (12 – 14%, see introduction) may arise for several reasons. We first assess the volatility of
 759 assumed first- and second-generation products using group contribution theory in order to
 760 predict partitioning. After a single oxidation step, with a representative product assumed to be a

761 C₅ hydroperoxynitrate, the saturation vapor pressure estimated by group contribution theory
762 (Pankow and Asher 2008) at 283 K would be 2.10×10^{-3} Torr ($C^* = 1.7 \times 10^4 \mu\text{g m}^{-3}$ for MW =
763 147 g mol^{-1}), while a double-oxidized isoprene molecule (assuming a C₅ dihydroxy dinitrate) has
764 an estimated vapor pressure of 7.95×10^{-8} Torr ($C^* = 1.01 \mu\text{g m}^{-3}$ for MW = 226 g mol^{-1}). This
765 supports the conclusion that while the first oxidation step produces compounds too volatile to
766 contribute appreciably to aerosol formation, oxidizing both double bonds of the isoprene
767 molecule is sufficient to produce substantial partitioning, consistent with Rollins et al. (Rollins et
768 al., 2009). This is also true if the second double bond is not oxidized by nitrate (group
769 contribution estimate P_{vap} for a C₅ tri-hydroxy nitrate is 7.7×10^{-8} Torr, $C^* = 0.79 \mu\text{g m}^{-3}$ for MW =
770 181 g mol^{-1}). These C^* saturation concentration values suggest that no dimer formation or
771 oligomerization is *required* to produce low-enough volatility products to condense to the aerosol
772 phase; however, such oligomerization would result in more efficient condensation. The fact that
773 Rollins et al. (Rollins et al., 2009) did not observe larger mass yields may indicate that it takes
774 longer than a typical chamber experiment timescale to reach equilibrium, or that this absorptive
775 partitioning model did not accurately capture those experiments, or that substantial loss of
776 semivolatiles to the chamber walls (e.g. (Krechmer et al., 2016)) suppressed apparent yields.
777

778 Determination of yields from ambient atmospheric data differs from chamber determinations in
779 several additional respects. First, ambient measurements do not suffer from wall loss effects,
780 such that no corrections are necessary for loss of aerosol or semi-volatile gases (Matsunaga
781 and Ziemann 2010, Krechmer et al., 2016). Second, ambient measurements take place on the
782 aging time scale of the atmosphere rather than a time scale imposed by the characteristics of
783 the chamber or the choice of oxidant addition. Third, the typical lifetime of the initially produced
784 nitrooxy-isoprene-RO₂ radical is more representative of the ambient atmosphere rather than a
785 chamber. The unique conditions of a high NO_x power plant plume affect lifetime and fates of
786 peroxy radicals, as described below.
787

788 To help interpret these in-plume peroxy radical lifetimes, a box model calculation using the
789 MCM v3.3.1 chemistry scheme was run (see details in Supplemental Information). This box
790 model shows substantially longer peroxy radical lifetimes during nighttime than daytime,
791 initializing with identical plume-observed conditions. These long peroxy radical lifetimes may
792 have consequences for comparison to chamber experiments: for example, in Schwantes'
793 (Schwantes et al., 2015) chamber experiment on the NO₃ + isoprene reaction mechanism, the
794 HO₂-limited nitrooxy-RO₂ lifetime was at maximum 30 s. In the plumes investigated in this study,
795 peroxy radical lifetimes are predicted to be substantially longer (>200 s early in the night, see
796 Fig. 7), allowing for the possibility of different bimolecular fates, or of unimolecular
797 transformations of the peroxy radicals that may result in lower-volatility products (e.g., auto-
798 oxidation to form highly oxidized molecules (Ehn et al., 2014)).
799

800



801
 802 **Figure 7.** Simulated peroxy radical concentration (left), loss rates (middle), and lifetime (right),
 803 using the MCM v3.3.1 chemical mechanism, for conditions typical of a nighttime intercepted
 804 power plant plume (top) and the same plume initial conditions run for daytime simulation
 805 (bottom, local noon occurs at 5 hrs). Included are total peroxy radical concentration and losses,
 806 as well as the highlighted subclasses HO_2 , CH_3O_2 , total nitrooxy-isoprene- RO_2 , and the total
 807 hydroxy-isoprene- RO_2 produced from OH oxidation. The righthand panels show HO_2 , CH_3O_2
 808 and the dominant hydroxy-isoprene- RO_2 ISOPBO_2 and ISOPDO_2 (β -hydroxy-peroxy radicals
 809 from OH attack at carbons 1 and 4 respectively) lifetime on the left axis and nitrooxy-isoprene-
 810 RO_2 on the right axis, showing nighttime lifetimes an order of magnitude longer than daytime for
 811 this NO_3 + isoprene derived RO_2 radical (NISOPPO_2).
 812

813 The typically assumed major fate of nighttime RO_2 in the atmosphere is reaction with HO_2 to
 814 yield a hydroperoxide, $\text{NO}_3\text{-ROOH}$. This is shown in the model output above as the green
 815 reaction, and is responsible for half of early RO_2 losses in the MCM modeled plume. Schwantes
 816 *et al.* (Schwantes *et al.*, 2015) proposed reaction of these nighttime derived hydroperoxides with
 817 OH during the following day as a route to epoxides, which in turn can form SOA via reaction
 818 with acidic aerosol. Reaction of hydroperoxides with nighttime generated OH may similarly
 819 provide a route to SOA through epoxides, albeit more slowly than that due to photochemically
 820 generated OH.
 821

822 The predicted longer nighttime peroxy radical lifetimes may enable unique chemistry. For
 823 example, if nitrooxy-isoprene- RO_2 self-reactions are substantially faster than assumed in the
 824 MCM, as suggested by Schwantes *et al.* (Schwantes *et al.*, 2015), $\text{RO}_2 + \text{RO}_2$ reactions may
 825 compete with the HO_2 reaction even more than shown in Fig. 7, and dimer formation may be
 826 favored at night, yielding lower volatility products. The 5:1 AMS Organic:Nitrate ratio observed in

827 the SOA formed in Rollins et al. (Rollins et al., 2009) , and consistent with aggregated
828 observations reported here, may suggest that in some isoprene units the nitrate is re-released
829 as NO₂ in such oligomerization reactions. We note that this larger organic to nitrate ratio would
830 mean higher SOA mass yields than estimated in Table 2.

831
832 Alternatively, longer nighttime peroxy radical lifetimes may allow sufficient time for
833 intramolecular reactions to produce condensable products. This unimolecular isomerization
834 (auto-oxidation) of initially formed peroxy radicals is a potentially efficient route to low-volatility,
835 highly functionalized products that could result in high aerosol yields. For OH-initiated oxidation
836 of isoprene, laboratory relative rate experiments found the fastest 1,6-H-shift isomerization
837 reaction to occur for the hydroxy-isoprene-RO₂ radical at a rate of 0.002 s⁻¹ (Crouse et al.,
838 2011), meaning that peroxy radicals must have an ambient lifetime of >500 s for this process to
839 be dominant. As shown in Fig. 7, the simulated power plant plume peroxy radical lifetimes are
840 long (>200 s), so an isomerization reaction at this rate may play a significant role. However, a
841 recent study has demonstrated that OH-initiated and NO₃-initiated RO₂ radicals from the same
842 precursor VOC can have very different unimolecular reactive fates due to highly structurally
843 sensitive varying rates of reactions of different product channels (Kurtén et al., 2017). A similar
844 theoretical study on the rate of unimolecular autooxidation reactions of nitrooxy-isoprene-RO₂
845 radicals would be valuable to help determine under what conditions such reactions might occur,
846 and this knowledge could be applied to comparing chamber and field SOA yields.

847 **4.4 Atmospheric implications and needs for future work**

848 Because this paper proposes higher SOA yield for the NO₃ + isoprene reaction than measured
849 in chamber studies, we conclude with some discussion of the implications for regional aerosol
850 burdens, and further needs for investigation in the NO₃ + isoprene system.

851
852 Using an isoprene + NO₃ yield parameterization that gave a 12% SOA mass yield at 10 µg m⁻³,
853 Pye et al. (2010) found that adding the NO₃ + isoprene oxidation pathway increased isoprene
854 SOA mass concentrations in the southeastern United States by about 30%, increases of 0.4 to
855 0.6 µg m⁻³. The larger NO₃ + isoprene SOA mass yields suggested in this paper, with average
856 value of 30%, could double this expected NO₃ radical enhancement of SOA production.
857 Edwards et al. (2017) concluded that the southeast U.S. is currently in transition between NO_x-
858 independent and NO_x-controlled nighttime BVOC oxidation regime. If NO₃-isoprene oxidation is
859 a larger aerosol source than currently understood, and if future NO_x reductions lead to a
860 stronger sensitivity in nighttime BVOC oxidation rates, regional SOA loadings could decrease by
861 a substantial fraction from the typical regional summertime OA loadings of 5 +/- 3 µg m⁻³ (Saha
862 et al., 2017).

863
864 Analysis of the degree of oxidation and chemical composition of NO₃ + isoprene SOA would
865 help to elucidate mechanistic reasons for the different field and lab SOA yields. For example,
866 the potential contribution of the uptake of morning-after OH + NISOPOOH produced epoxides,
867 discussed above in section 4.3, onto existing (acidic) aerosol could be quantified by
868 measurement of these intermediates or their products in the aerosol phase. Assessment of
869 degree of oxidation could help determine whether auto-oxidation mechanisms are active.

870 Because of the potentially large effect on predicted SOA loading in regions of high isoprene
871 emissions, a better mechanistic understanding of these observed yields is crucial.

872

873 **Acknowledgements**

874 JLF gratefully acknowledges funding from the EPA STAR Program (no. RD-83539901) and from
875 the Fulbright U.S. Scholars Program in the Netherlands. PCJ, DAD, and JLJ were partially
876 supported by EPA STAR 83587701-0 and DOE (BER/ASR) DE-SC0016559. This paper has not
877 been formally reviewed by EPA. The views expressed in this document are solely those of the
878 authors, and do not necessarily reflect those of EPA. EPA does not endorse any products or
879 commercial services mentioned in this publication.

880 **5 References**

- 881 Allan, J. D., K. N. Bower, H. Coe, H. Boudries, J. T. Jayne, M. R. Canagaratna, D. B. Millet, A.
882 H. Goldstein, P. K. Quinn, R. J. Weber and D. R. Worsnop (2004). "Submicron aerosol
883 composition at Trinidad Head, California, during ITCT 2K2: Its relationship with gas phase
884 volatile organic carbon and assessment of instrument performance." Journal of Geophysical
885 Research: Atmospheres **109**(D23): n/a-n/a.
- 886 Allan, J. D., A. E. Delia, H. Coe, K. N. Bower, M. R. Alfarra, J. L. Jimenez, A. M. Middlebrook, F.
887 Drewnick, T. B. Onasch, M. R. Canagaratna, J. T. Jayne and D. R. Worsnop (2004). "A
888 generalised method for the extraction of chemically resolved mass spectra from Aerodyne
889 aerosol mass spectrometer data." Journal of Aerosol Science **35**(7): 909-922.
- 890 Atkinson, R., D. L. Baulch, R. A. Cox, J. N. Crowley, R. F. Hampson, R. G. Hynes, M. E. Jenkin,
891 M. J. Rossi and J. Troe (2004). "Evaluated kinetic and photochemical data for atmospheric
892 chemistry: Volume I - gas phase reactions of Ox, HOx, NOx and SOx species." Atmos. Chem.
893 Phys. **4**(6): 1461-1738.
- 894 Ayres, B. R., H. M. Allen, D. C. Draper, S. S. Brown, R. J. Wild, J. L. Jimenez, D. A. Day, P.
895 Campuzano-Jost, W. Hu, J. de Gouw, A. Koss, R. C. Cohen, K. C. Duffey, P. Romer, K.
896 Baumann, E. Edgerton, S. Takahama, J. A. Thornton, B. H. Lee, F. D. Lopez-Hilfiker, C. Mohr,
897 P. O. Wennberg, T. B. Nguyen, A. Teng, A. H. Goldstein, K. Olson and J. L. Fry (2015).
898 "Organic nitrate aerosol formation via NO₃ + biogenic volatile organic compounds
899 in the southeastern United States." Atmos. Chem. Phys. **15**(23): 13377-13392.
- 900 Bahreini, R., E. J. Dunlea, B. M. Matthew, C. Simons, K. S. Docherty, P. F. DeCarlo, J. L.
901 Jimenez, C. A. Brock and A. M. Middlebrook (2008). "Design and Operation of a Pressure-
902 Controlled Inlet for Airborne Sampling with an Aerodynamic Aerosol Lens." Aerosol Science and
903 Technology **42**(6): 465-471.
- 904 Bahreini, R., B. Ervens, A. M. Middlebrook, C. Warneke, J. A. de Gouw, P. F. DeCarlo, J. L.
905 Jimenez, C. A. Brock, J. A. Neuman, T. B. Ryerson, H. Stark, E. Atlas, J. Brioude, A. Fried, J. S.
906 Holloway, J. Peischl, D. Richter, J. Walega, P. Weibring, A. G. Wollny and F. C. Fehsenfeld
907 (2009). "Organic aerosol formation in urban and industrial plumes near Houston and Dallas,
908 Texas." Journal of Geophysical Research: Atmospheres **114**(D7): n/a-n/a.
- 909 Boyd, C. M., J. Sanchez, L. Xu, A. J. Eugene, T. Nah, W. Y. Tuet, M. I. Guzman and N. L. Ng
910 (2015). "Secondary organic aerosol formation from the β -pinene+NO₃ system: effect of humidity
911 and peroxy radical fate." Atmos. Chem. Phys. **15**(13): 7497-7522.
- 912 Brock, C. A., J. Cozic, R. Bahreini, K. D. Froyd, A. M. Middlebrook, A. McComiskey, J. Brioude,
913 O. R. Cooper, A. Stohl, K. C. Aikin, J. A. de Gouw, D. W. Fahey, R. A. Ferrare, R. S. Gao, W.
914 Gore, J. S. Holloway, G. Hübler, A. Jefferson, D. A. Lack, S. Lance, R. H. Moore, D. M. Murphy,
915 A. Nenes, P. C. Novelli, J. B. Nowak, J. A. Ogren, J. Peischl, R. B. Pierce, P. Pilewskie, P. K.
916 Quinn, T. B. Ryerson, K. S. Schmidt, J. P. Schwarz, H. Sodemann, J. R. Spackman, H. Stark,

917 D. S. Thomson, T. Thornberry, P. Veres, L. A. Watts, C. Warneke and A. G. Wollny (2011).
918 "Characteristics, sources, and transport of aerosols measured in spring 2008 during the aerosol,
919 radiation, and cloud processes affecting Arctic Climate (ARCPAC) Project." Atmos. Chem.
920 Phys. **11**(6): 2423-2453.

921 Brock, C. A., N. L. Wagner, B. E. Anderson, A. R. Attwood, A. Beyersdorf, P. Campuzano-Jost,
922 A. G. Carlton, D. A. Day, G. S. Diskin, T. D. Gordon, J. L. Jimenez, D. A. Lack, J. Liao, M. Z.
923 Markovic, A. M. Middlebrook, N. L. Ng, A. E. Perring, M. S. Richardson, J. P. Schwarz, R. A.
924 Washenfelder, A. Welti, L. Xu, L. D. Ziemba and D. M. Murphy (2016). "Aerosol optical
925 properties in the southeastern United States in summer – Part 1: Hygroscopic growth." Atmos.
926 Chem. Phys. **16**(8): 4987-5007.

927 Brown, S. S., J. A. deGouw, C. Warneke, T. B. Ryerson, W. P. Dubé, E. Atlas, R. J. Weber, R.
928 E. Peltier, J. A. Neuman, J. M. Roberts, A. Swanson, F. Flocke, S. A. McKeen, J. Brioude, R.
929 Sommariva, M. Trainer, F. C. Fehsenfeld and A. R. Ravishankara (2009). "Nocturnal isoprene
930 oxidation over the Northeast United States in summer and its impact on reactive nitrogen
931 partitioning and secondary organic aerosol." Atmos. Chem. Phys. **9**(9): 3027-3042.

932 Brown, S. S., W. P. Dubé, R. Bahreini, A. M. Middlebrook, C. A. Brock, C. Warneke, J. A. de
933 Gouw, R. A. Washenfelder, E. Atlas, J. Peischl, T. B. Ryerson, J. S. Holloway, J. P. Schwarz, R.
934 Spackman, M. Trainer, D. D. Parrish, F. C. Fehshenfeld and A. R. Ravishankara (2013).
935 "Biogenic VOC oxidation and organic aerosol formation in an urban nocturnal boundary layer:
936 aircraft vertical profiles in Houston, TX." Atmos. Chem. Phys. **13**(22): 11317-11337.

937 Brown, S. S., W. P. Dubé, P. Karamchandani, G. Yarwood, J. Peischl, T. B. Ryerson, J. A.
938 Neuman, J. B. Nowak, J. S. Holloway, R. A. Washenfelder, C. A. Brock, G. J. Frost, M. Trainer,
939 D. D. Parrish, F. C. Fehsenfeld and A. R. Ravishankara (2012). "Effects of NO_x control and
940 plume mixing on nighttime chemical processing of plumes from coal-fired power plants." Journal
941 of Geophysical Research: Atmospheres **117**(D7): n/a-n/a.

942 Brown, S. S., J. A. Neuman, T. B. Ryerson, M. Trainer, W. P. Dubé, J. S. Holloway, C.
943 Warneke, J. A. de Gouw, S. G. Donnelly, E. Atlas, B. Matthew, A. M. Middlebrook, R. Peltier, R.
944 J. Weber, A. Stohl, J. F. Meagher, F. C. Fehsenfeld and A. R. Ravishankara (2006). "Nocturnal
945 odd-oxygen budget and its implications for ozone loss in the lower troposphere." Geophysical
946 Research Letters **33**(8): n/a-n/a.

947 Brown, S. S. and J. Stutz (2012). "Nighttime radical observations and chemistry." Chemical
948 Society Reviews **41**(19): 6405-6447.

949 Bruns, E. A., V. Perraud, A. Zelenyuk, M. J. Ezell, S. N. Johnson, Y. Yu, D. Imre, B. J.
950 Finlayson-Pitts and M. L. Alexander (2010). "Comparison of FTIR and Particle Mass
951 Spectrometry for the Measurement of Particulate Organic Nitrates." Environmental Science &
952 Technology **44**(3): 1056-1061.

953 Cai, Y., D. C. Montague, W. Mooiweer-Bryan and T. Deshler (2008). Performance
954 characteristics of the ultra high sensitivity aerosol spectrometer for particles between 55 and
955 800 nm: Laboratory and field studies.

956 Calvert, J. G., J. A. Atkinson, J. A. Kerr, S. Madronich, G. K. Moortgat, T. J. Wallington and G.
957 Yarwood (2000). Mechanisms of the atmospheric oxidation of the alkenes. New York, NY,
958 Oxford University Press.

959 Carlton, A. G., R. W. Pinder, P. V. Bhave and G. A. Pouliot (2010). "To What Extent Can
960 Biogenic SOA be Controlled?" Environmental Science & Technology **44**(9): 3376-3380.

961 Carlton, A. G., C. Wiedinmyer and J. H. Kroll (2009). "A review of Secondary Organic Aerosol
962 (SOA) formation from isoprene." Atmos. Chem. Phys. **9**(14): 4987-5005.

963 Crouse, J. D., F. Paulot, H. G. Kjaergaard and P. O. Wennberg (2011). "Peroxy radical
964 isomerization in the oxidation of isoprene." Physical Chemistry Chemical Physics **13**(30): 13607-
965 13613.

966 D'Ambro, E. L., K. H. Møller, F. D. Lopez-Hilfiker, S. Schobesberger, J. Liu, J. E. Shilling, B. H.
967 Lee, H. G. Kjaergaard and J. A. Thornton (2017). "Isomerization of Second-Generation Isoprene

968 Peroxy Radicals: Epoxide Formation and Implications for Secondary Organic Aerosol Yields." *Environmental Science & Technology* **51**(9): 4978-4987.

969

970 Darer, A. I., N. C. Cole-Filipiak, A. E. O'Connor and M. J. Elrod (2011). "Formation and Stability

971 of Atmospherically Relevant Isoprene-Derived Organosulfates and Organonitrates."

972 *Environmental Science & Technology* **45**(5): 1895-1902.

973 Day, D. A., P. Campuzano-Jost, B. B. Palm, W. W. Hu, B. A. Nault, P. J. Wooldridge, R. C.

974 Cohen, K. S. Docherty, J. A. Huffman and J. L. Jimenez (2017). "Evaluation of methods for

975 quantification of bulk particle-phase organic nitrates using real-time aerosol mass spectrometry."

976 *in preparation*.

977 Dommen, J., H. Hellén, M. Saurer, M. Jaeggi, R. Siegwolf, A. Metzger, J. Duplissy, M. Fierz and

978 U. Baltensperger (2009). "Determination of the Aerosol Yield of Isoprene in the Presence of an

979 Organic Seed with Carbon Isotope Analysis." *Environmental Science & Technology* **43**(17):

980 6697-6702.

981 Drewnick, F., S. S. Hings, P. DeCarlo, J. T. Jayne, M. Gonin, K. Fuhrer, S. Weimer, J. L.

982 Jimenez, K. L. Demerjian, S. Borrmann and D. R. Worsnop (2005). "A New Time-of-Flight

983 Aerosol Mass Spectrometer (TOF-AMS)—Instrument Description and First Field Deployment."

984 *Aerosol Science and Technology* **39**(7): 637-658.

985 Dunlea, E. J., P. F. DeCarlo, A. C. Aiken, J. R. Kimmel, R. E. Peltier, R. J. Weber, J. Tomlinson,

986 D. R. Collins, Y. Shinozuka, C. S. McNaughton, S. G. Howell, A. D. Clarke, L. K. Emmons, E. C.

987 Apel, G. G. Pfister, A. van Donkelaar, R. V. Martin, D. B. Millet, C. L. Heald and J. L. Jimenez

988 (2009). "Evolution of Asian aerosols during transpacific transport in INTEX-B." *Atmos. Chem.*

989 *Phys.* **9**(19): 7257-7287.

990 Edwards, P. M., K. C. Aikin, W. P. Dube, J. L. Fry, J. B. Gilman, J. A. de Gouw, M. G. Graus, T.

991 F. Hanisco, J. Holloway, G. Hubler, J. Kaiser, F. N. Keutsch, B. M. Lerner, J. A. Neuman, D. D.

992 Parrish, J. Peischl, I. B. Pollack, A. R. Ravishankara, J. M. Roberts, T. B. Ryerson, M. Trainer,

993 P. R. Veres, G. M. Wolfe, C. Warneke and S. S. Brown (2017). "Transition from high- to low-

994 NO_x control of night-time oxidation in the southeastern US." *Nature Geosci* **10**(7): 490-495.

995 Ehn, M., J. A. Thornton, E. Kleist, M. Sipila, H. Junninen, I. Pullinen, M. Springer, F. Rubach, R.

996 Tillmann, B. Lee, F. Lopez-Hilfiker, S. Andres, I.-H. Acir, M. Rissanen, T. Jokinen, S.

997 Schobesberger, J. Kangasluoma, J. Kontkanen, T. Nieminen, T. Kurten, L. B. Nielsen, S.

998 Jorgensen, H. G. Kjaergaard, M. Canagaratna, M. D. Maso, T. Berndt, T. Petaja, A. Wahner, V.-

999 M. Kerminen, M. Kulmala, D. R. Worsnop, J. Wildt and T. F. Mentel (2014). "A large source of

1000 low-volatility secondary organic aerosol." *Nature* **506**(7489): 476-479.

1001 Emmerson, K. M. and M. J. Evans (2009). "Comparison of tropospheric gas-phase chemistry

1002 schemes for use within global models." *Atmos. Chem. Phys.* **9**(5): 1831-1845.

1003 Farmer, D. K., A. Matsunaga, K. S. Docherty, J. D. Surratt, J. H. Seinfeld, P. J. Ziemann and J.

1004 L. Jimenez (2010). "Response of an aerosol mass spectrometer to organonitrates and

1005 organosulfates and implications for atmospheric chemistry." *Proceedings of the National*

1006 *Academy of Sciences* **107**(15): 6670-6675.

1007 Fisher, J. A., D. J. Jacob, K. R. Travis, P. S. Kim, E. A. Marais, C. Chan Miller, K. Yu, L. Zhu, R.

1008 M. Yantosca, M. P. Sulprizio, J. Mao, P. O. Wennberg, J. D. Crouse, A. P. Teng, T. B. Nguyen,

1009 J. M. St. Clair, R. C. Cohen, P. Romer, B. A. Nault, P. J. Wooldridge, J. L. Jimenez, P.

1010 Campuzano-Jost, D. A. Day, W. Hu, P. B. Shepson, F. Xiong, D. R. Blake, A. H. Goldstein, P.

1011 K. Misztal, T. F. Hanisco, G. M. Wolfe, T. B. Ryerson, A. Wisthaler and T. Mikoviny (2016).

1012 "Organic nitrate chemistry and its implications for nitrogen budgets in an isoprene- and

1013 monoterpene-rich atmosphere: constraints from aircraft (SEAC4RS) and ground-based (SOAS)

1014 observations in the Southeast US." *Atmos. Chem. Phys.* **16**(9): 5969-5991.

1015 Fry, J. L., D. C. Draper, K. J. Zarzana, P. Campuzano-Jost, D. A. Day, J. L. Jimenez, S. S.

1016 Brown, R. C. Cohen, L. Kaser, A. Hansel, L. Cappellin, T. Karl, A. Hodzic Roux, A. Turnipseed,

1017 C. Cantrell, B. L. Lefer and N. Grossberg (2013). "Observations of gas- and aerosol-phase

1018 organic nitrates at BEACHON-RoMBAS 2011." *Atmos. Chem. Phys.* **13**(1): 8585-8605.

1019 Fry, J. L., A. Kiendler-Scharr, A. W. Rollins, T. Brauers, S. S. Brown, H.-P. Dorn, W. P. Dube, H.
1020 Fuchs, A. Mensah, F. Rohrer, R. Tillmann, A. Wahner, P. J. Wooldridge and R. C. Cohen
1021 (2011). "SOA from limonene: role of NO₃ in its generation and degradation." Atmospheric
1022 Chemistry and Physics **11**(8): 3879-3894.

1023 Fry, J. L., A. Kiendler-Scharr, A. W. Rollins, P. J. Wooldridge, S. S. Brown, H. Fuchs, W. Dube,
1024 A. Mensah, M. dal Maso, R. Tillmann, H. P. Dorn, T. Brauers and R. C. Cohen (2009). "Organic
1025 nitrate and secondary organic aerosol yield from NO₃ oxidation of beta-pinene evaluated using
1026 a gas-phase kinetics/aerosol partitioning model." Atmospheric Chemistry and Physics **9**(4):
1027 1431-1449.

1028 Fry, J. L., C. Koski, K. Bott, R. Hsu-Flanders and M. Hazell (2015). "Downwind particulate
1029 matters: Regulatory implications of secondary aerosol formation from the interaction of nitrogen
1030 oxides and tree emissions." Environmental Science & Policy **50**: 180-190.

1031 Goldstein, A. H., C. D. Koven, C. L. Heald and I. Y. Fung (2009). "Biogenic carbon and
1032 anthropogenic pollutants combine to form a cooling haze over the southeastern United States."
1033 Proceedings of the National Academy of Sciences **106**(22): 8835-8840.

1034 Guenther, A., T. Karl, P. Harley, C. Wiedinmyer, P. I. Palmer and C. Geron (2006). "Estimates
1035 of global terrestrial isoprene emissions using MEGAN (Model of Emissions of Gases and
1036 Aerosols from Nature)." Atmos. Chem. Phys **6**: 3181-3210.

1037 Guo, H., L. Xu, A. Bougiatioti, K. M. Cerully, S. L. Capps, J. R. Hite Jr, A. G. Carlton, S. H. Lee,
1038 M. H. Bergin, N. L. Ng, A. Nenes and R. J. Weber (2015). "Fine-particle water and pH in the
1039 southeastern United States." Atmos. Chem. Phys. **15**(9): 5211-5228.

1040 Hallquist, M., J. C. Wenger, U. Baltensperger, Y. Rudich, D. Simpson, M. Claeys, J. Dommen,
1041 N. M. Donahue, C. George, A. H. Goldstein, J. F. Hamilton, H. Herrmann, T. Hoffmann, Y.
1042 Iinuma, M. Jang, M. E. Jenkin, J. L. Jimenez, A. Kiendler-Scharr, W. Maenhaut, G. McFiggans,
1043 T. F. Mentel, A. Monod, A. S. H. Prévôt, J. H. Seinfeld, J. D. Surratt, R. Szmigielski and J. Wildt
1044 (2009). "The formation, properties and impact of secondary organic aerosol: current and
1045 emerging issues." Atmospheric Chemistry & Physics **9**: 5155-5235.

1046 Hayes, P. L., A. M. Ortega, M. J. Cubison, K. D. Froyd, Y. Zhao, S. S. Cliff, W. W. Hu, D. W.
1047 Toohey, J. H. Flynn, B. L. Lefer, N. Grossberg, S. Alvarez, B. Rappenglück, J. W. Taylor, J. D.
1048 Allan, J. S. Holloway, J. B. Gilman, W. C. Kuster, J. A. de Gouw, P. Massoli, X. Zhang, J. Liu, R.
1049 J. Weber, A. L. Corrigan, L. M. Russell, G. Isaacman, D. R. Worton, N. M. Kreisberg, A. H.
1050 Goldstein, R. Thalman, E. M. Waxman, R. Volkamer, Y. H. Lin, J. D. Surratt, T. E. Kleindienst,
1051 J. H. Offenberg, S. Dusanter, S. Griffith, P. S. Stevens, J. Brioude, W. M. Angevine and J. L.
1052 Jimenez (2013). "Organic aerosol composition and sources in Pasadena, California, during the
1053 2010 CalNex campaign." Journal of Geophysical Research: Atmospheres **118**(16): 9233-9257.

1054 Heald, C. L., D. K. Henze, L. W. Horowitz, J. Feddema, J. F. Lamarque, A. Guenther, P. G.
1055 Hess, F. Vitt, J. H. Seinfeld, A. H. Goldstein and I. Fung (2008). "Predicted change in global
1056 secondary organic aerosol concentrations in response to future climate, emissions, and land
1057 use change." Journal of Geophysical Research: Atmospheres **113**(D5): n/a-n/a.

1058 Henze, D. K. and J. H. Seinfeld (2006). "Global secondary organic aerosol from isoprene
1059 oxidation." Geophysical Research Letters **33**(9).

1060 Hoyle, C., M. Boy, N. Donahue, J. Fry, M. Glasius, A. Guenther, A. Hallar, K. H. Hartz, M.
1061 Petters and T. Petaja (2011). "A review of the anthropogenic influence on biogenic secondary
1062 organic aerosol." Atmospheric Chemistry and Physics **11**(1): 321-343.

1063 Hoyle, C. R., T. Berntsen, G. Myhre and I. S. A. Isaksen (2007). "Secondary organic aerosol in
1064 the global aerosol - chemical transport model Oslo CTM2." Atmospheric Chemistry and Physics
1065 **7**(21): 5675-5694.

1066 Hu, K. S., A. I. Darer and M. J. Elrod (2011). "Thermodynamics and kinetics of the hydrolysis of
1067 atmospherically relevant organonitrates and organosulfates." Atmos. Chem. Phys. **11**(16): 8307-
1068 8320.

1069 Hu, W. W., P. Campuzano-Jost, B. B. Palm, D. A. Day, A. M. Ortega, P. L. Hayes, J. E.
1070 Krechmer, Q. Chen, M. Kuwata, Y. J. Liu, S. S. de Sá, K. McKinney, S. T. Martin, M. Hu, S. H.
1071 Budisulistiorini, M. Riva, J. D. Surratt, J. M. St. Clair, G. Isaacman-Van Wertz, L. D. Yee, A. H.
1072 Goldstein, S. Carbone, J. Brito, P. Artaxo, J. A. de Gouw, A. Koss, A. Wisthaler, T. Mikoviny, T.
1073 Karl, L. Kaser, W. Jud, A. Hansel, K. S. Docherty, M. L. Alexander, N. H. Robinson, H. Coe, J.
1074 D. Allan, M. R. Canagaratna, F. Paulot and J. L. Jimenez (2015). "Characterization of a real-
1075 time tracer for isoprene epoxydiols-derived secondary organic aerosol (IEPOX-SOA) from
1076 aerosol mass spectrometer measurements." *Atmos. Chem. Phys.* **15**(20): 11807-11833.
1077 Jenkin, M. E., J. C. Young and A. R. Rickard (2015). "The MCM v3.3.1 degradation scheme for
1078 isoprene." *Atmos. Chem. Phys.* **15**(20): 11433-11459.
1079 Jimenez, J. L., M. R. Canagaratna, N. M. Donahue, A. S. H. Prevot, Q. Zhang, J. H. Kroll, P. F.
1080 DeCarlo, J. D. Allan, H. Coe, N. L. Ng, A. C. Aiken, K. S. Docherty, I. M. Ulbrich, A. P. Grieshop,
1081 A. L. Robinson, J. Duplissy, J. D. Smith, K. R. Wilson, V. A. Lanz, C. Hueglin, Y. L. Sun, J. Tian,
1082 A. Laaksonen, T. Raatikainen, J. Rautiainen, P. Vaattovaara, M. Ehn, M. Kulmala, J. M.
1083 Tomlinson, D. R. Collins, M. J. Cubison, E., J. Dunlea, J. A. Huffman, T. B. Onasch, M. R.
1084 Alfarra, P. I. Williams, K. Bower, Y. Kondo, J. Schneider, F. Drewnick, S. Borrmann, S. Weimer,
1085 K. Demerjian, D. Salcedo, L. Cottrell, R. Griffin, A. Takami, T. Miyoshi, S. Hatakeyama, A.
1086 Shimono, J. Y. Sun, Y. M. Zhang, K. Dzepina, J. R. Kimmel, D. Sueper, J. T. Jayne, S. C.
1087 Herndon, A. M. Trimborn, L. R. Williams, E. C. Wood, A. M. Middlebrook, C. E. Kolb, U.
1088 Baltensperger and D. R. Worsnop (2009). "Evolution of Organic Aerosols in the Atmosphere."
1089 *Science*(5959): 1525-1529.
1090 Kanakidou, M., J. H. Seinfeld, S. N. Pandis, I. Barnes, F. J. Dentener, M. C. Facchini, R. Van
1091 Dingenen, B. Ervens, A. Nenes, C. J. Nielsen, E. Swietlicki, J. P. Putaud, Y. Balkanski, S. Fuzzi,
1092 J. Horth, G. K. Moortgat, R. Winterhalter, C. E. L. Myhre, K. Tsigaridis, E. Vignati, E. G.
1093 Stephanou and J. Wilson (2005). "Organic aerosol and global climate modelling: a review."
1094 *Atmospheric Chemistry and Physics* **5**: 1053-1123.
1095 Kiendler-Scharr, A., A. A. Mensah, E. Friese, D. Topping, E. Nemitz, A. S. H. Prevot, M. Äijälä,
1096 J. Allan, F. Canonaco, M. Canagaratna, S. Carbone, M. Crippa, M. Dall'Osto, D. A. Day, P. De
1097 Carlo, C. F. Di Marco, H. Elbern, A. Eriksson, E. Freney, L. Hao, H. Herrmann, L. Hildebrandt,
1098 R. Hillamo, J. L. Jimenez, A. Laaksonen, G. McFiggans, C. Mohr, C. O'Dowd, R. Otjes, J.
1099 Ovadnevaite, S. N. Pandis, L. Poulain, P. Schlag, K. Sellegri, E. Swietlicki, P. Tiitta, A.
1100 Vermeulen, A. Wahner, D. Worsnop and H. C. Wu (2016). "Ubiquity of organic nitrates from
1101 nighttime chemistry in the European submicron aerosol." *Geophysical Research Letters* **43**(14):
1102 7735-7744.
1103 Kim, P. S., D. J. Jacob, J. A. Fisher, K. Travis, K. Yu, L. Zhu, R. M. Yantosca, M. P. Sulprizio, J.
1104 L. Jimenez, P. Campuzano-Jost, K. D. Froyd, J. Liao, J. W. Hair, M. A. Fenn, C. F. Butler, N. L.
1105 Wagner, T. D. Gordon, A. Welti, P. O. Wennberg, J. D. Crouse, J. M. St. Clair, A. P. Teng, D.
1106 B. Millet, J. P. Schwarz, M. Z. Markovic and A. E. Perring (2015). "Sources, seasonality, and
1107 trends of southeast US aerosol: an integrated analysis of surface, aircraft, and satellite
1108 observations with the GEOS-Chem chemical transport model." *Atmos. Chem. Phys.* **15**(18):
1109 10411-10433.
1110 Kleindienst, T. E., M. Lewandowski, J. H. Offenberg, M. Jaoui and E. O. Edney (2007). "Ozone-
1111 isoprene reaction: Re-examination of the formation of secondary organic aerosol." *Geophysical*
1112 *Research Letters* **34**(1): n/a-n/a.
1113 Krechmer, J. E., D. Pagonis, P. J. Ziemann and J. L. Jimenez (2016). "Quantification of Gas-
1114 Wall Partitioning in Teflon Environmental Chambers Using Rapid Bursts of Low-Volatility
1115 Oxidized Species Generated in Situ." *Environmental Science & Technology* **50**(11): 5757-5765.
1116 Kroll, J. H., N. L. Ng, S. M. Murphy, R. C. Flagan and J. H. Seinfeld (2006). "Secondary Organic
1117 Aerosol Formation from Isoprene Photooxidation." *Environmental Science & Technology* **40**(6):
1118 1869-1877.

1119 Kurtén, T., K. H. Møller, T. B. Nguyen, R. H. Schwantes, P. K. Misztal, L. Su, P. O. Wennberg,
1120 J. L. Fry and H. G. Kjaergaard (2017). "Alkoxy Radical Bond Scissions Explain the Anomalously
1121 Low Secondary Organic Aerosol and Organonitrate Yields From α -Pinene + NO₃." The Journal
1122 of Physical Chemistry Letters: 2826-2834.

1123 Lee, B. H., C. Mohr, F. D. Lopez-Hilfiker, A. Lutz, M. Hallquist, L. Lee, P. Romer, R. C. Cohen,
1124 S. Iyer, T. Kurtén, W. Hu, D. A. Day, P. Campuzano-Jost, J. L. Jimenez, L. Xu, N. L. Ng, H.
1125 Guo, R. J. Weber, R. J. Wild, S. S. Brown, A. Koss, J. de Gouw, K. Olson, A. H. Goldstein, R.
1126 Seco, S. Kim, K. McAvey, P. B. Shepson, T. Starn, K. Baumann, E. S. Edgerton, J. Liu, J. E.
1127 Shilling, D. O. Miller, W. Brune, S. Schobesberger, E. L. D'Ambro and J. A. Thornton (2016).
1128 "Highly functionalized organic nitrates in the southeast United States: Contribution to secondary
1129 organic aerosol and reactive nitrogen budgets." Proceedings of the National Academy of
1130 Sciences **113**(6): 1516-1521.

1131 Lelieveld, J., J. S. Evans, M. Fnais, D. Giannadaki and A. Pozzer (2015). "The contribution of
1132 outdoor air pollution sources to premature mortality on a global scale." Nature **525**(7569): 367-
1133 371.

1134 Lerner, B. M., J. B. Gilman, K. C. Aikin, E. L. Atlas, P. D. Goldan, M. Graus, R. Hendershot, G.
1135 A. Isaacman-VanWertz, A. Koss, W. C. Kuster, R. A. Lueb, R. J. McLaughlin, J. Peischl, D.
1136 Sueper, T. B. Ryerson, T. W. Tokarek, C. Warneke, B. Yuan and J. A. de Gouw (2017). "An
1137 improved, automated whole air sampler and gas chromatography mass spectrometry analysis
1138 system for volatile organic compounds in the atmosphere." Atmos. Meas. Tech. **10**(1): 291-313.

1139 Liu, J., E. L. D'Ambro, B. H. Lee, F. D. Lopez-Hilfiker, R. A. Zaveri, J. C. Rivera-Rios, F. N.
1140 Keutsch, S. Iyer, T. Kurten, Z. Zhang, A. Gold, J. D. Surratt, J. E. Shilling and J. A. Thornton
1141 (2016). "Efficient Isoprene Secondary Organic Aerosol Formation from a Non-IEPOX Pathway."
1142 Environmental Science & Technology **50**(18): 9872-9880.

1143 Marais, E. A., D. J. Jacob, J. L. Jimenez, P. Campuzano-Jost, D. A. Day, W. Hu, J. Krechmer,
1144 L. Zhu, P. S. Kim, C. C. Miller, J. A. Fisher, K. Travis, K. Yu, T. F. Hanisco, G. M. Wolfe, H. L.
1145 Arkinson, H. O. T. Pye, K. D. Froyd, J. Liao and V. F. McNeill (2016). "Aqueous-phase
1146 mechanism for secondary organic aerosol formation from isoprene: application to the southeast
1147 United States and co-benefit of SO₂ emission controls." Atmos. Chem. Phys. **16**(3): 1603-1618.

1148 Marcolli, C., M. R. Canagaratna, D. R. Worsnop, R. Bahreini, J. A. de Gouw, C. Warneke, P. D.
1149 Goldan, W. C. Kuster, E. J. Williams, B. M. Lerner, J. M. Roberts, J. F. Meagher, F. C.
1150 Fehsenfeld, M. Marchewka, S. B. Bertman and A. M. Middlebrook (2006). "Cluster Analysis of
1151 the Organic Peaks in Bulk Mass Spectra Obtained During the 2002 New England Air Quality
1152 Study with an Aerodyne Aerosol Mass Spectrometer." Atmos. Chem. Phys. **6**(12): 5649-5666.

1153 Matsunaga, A. and P. J. Ziemann (2010). "Gas-Wall Partitioning of Organic Compounds in a
1154 Teflon Film Chamber and Potential Effects on Reaction Product and Aerosol Yield
1155 Measurements." Aerosol Science and Technology **44**(10): 881-892.

1156 Middlebrook, A. M., R. Bahreini, J. L. Jimenez and M. R. Canagaratna (2012). "Evaluation of
1157 Composition-Dependent Collection Efficiencies for the Aerodyne Aerosol Mass Spectrometer
1158 using Field Data." Aerosol Science and Technology **46**(3): 258-271.

1159 Myhre, G., D. Shindell, F.-M. Bréon, W. Collins, J. Fuglestedt, J. Huang, D. Koch, J.-F.
1160 Lamarque, D. Lee, B. Mendoza, T. Nakajima, A. Robock, G. Stephens, T. Takemura and H.
1161 Zhang (2013). Anthropogenic And Natural Radiative Forcing, in Climate Change 2013: The
1162 Physical Science Basis. Contribution of Working Group I to the Fifth Assessment Report of the
1163 Intergovernmental Panel on Climate Change. T. F. Stocker, D. Qin, G.-K. Plattner et al. New
1164 York, NY, USA, Cambridge University Press: 659-740.

1165 NASA. (2018). "SEAC4RS data site." from DOI: 10.5067/Aircraft/SEAC4RS/Aerosol-TraceGas-
1166 Cloud.

1167 Ng, N. L., S. S. Brown, A. T. Archibald, E. Atlas, R. C. Cohen, J. N. Crowley, D. A. Day, N. M.
1168 Donahue, J. L. Fry, H. Fuchs, R. J. Griffin, M. I. Guzman, H. Herrmann, A. Hodzic, Y. Iinuma, J.
1169 L. Jimenez, A. Kiendler-Scharr, B. H. Lee, D. J. Luecken, J. Mao, R. McLaren, A. Mutzel, H. D.

1170 Osthoff, B. Ouyang, B. Picquet-Varrault, U. Platt, H. O. T. Pye, Y. Rudich, R. H. Schwantes, M.
1171 Shiraiwa, J. Stutz, J. A. Thornton, A. Tilgner, B. J. Williams and R. A. Zaveri (2017). "Nitrate
1172 radicals and biogenic volatile organic compounds: oxidation, mechanisms, and organic aerosol."
1173 Atmos. Chem. Phys. **17**(3): 2103-2162.

1174 Ng, N. L., A. J. Kwan, J. D. Surratt, A. W. H. Chan, P. S. Chhabra, A. Sorooshian, H. O. T. Pye,
1175 J. D. Crouse, P. O. Wennberg, R. C. Flagan and J. H. Seinfeld (2008). "Secondary organic
1176 aerosol (SOA) formation from reaction of isoprene with nitrate radicals (NO₃)." Atmos. Chem.
1177 Phys. **8**: 4117-4140.

1178 Palm, B. B., P. Campuzano-Jost, D. A. Day, A. M. Ortega, J. L. Fry, S. S. Brown, K. J. Zarzana,
1179 W. Dube, N. L. Wagner, D. C. Draper, L. Kaser, W. Jud, T. Karl, A. Hansel, C. Gutiérrez-Montes
1180 and J. L. Jimenez (2017). "Secondary organic aerosol formation from in situ OH, O₃, and NO₃
1181 oxidation of ambient forest air in an oxidation flow reactor." Atmos. Chem. Phys. **17**(8): 5331-
1182 5354.

1183 Pankow, J. F. and W. E. Asher (2008). "SIMPOL.1: a simple group contribution method for
1184 predicting vapor pressures and enthalpies of vaporization of multifunctional organic
1185 compounds." Atmospheric Chemistry and Physics **8**(10): 2773-2796.

1186 Peischl, J., T. B. Ryerson, J. S. Holloway, D. D. Parrish, M. Trainer, G. J. Frost, K. C. Aikin, S.
1187 S. Brown, W. P. Dubé, H. Stark and F. C. Fehsenfeld (2010). "A top-down analysis of emissions
1188 from selected Texas power plants during TexAQS 2000 and 2006." Journal of Geophysical
1189 Research: Atmospheres **115**(D16): n/a-n/a.

1190 Pye, H., A. Chan, M. Barkley and J. Seinfeld (2010). "Global modeling of organic aerosol: the
1191 importance of reactive nitrogen (NO_x and NO₃)." Atmospheric Chemistry and Physics **10**(22):
1192 11261-11276.

1193 Pye, H. O. T., D. J. Luecken, L. Xu, C. M. Boyd, N. L. Ng, K. R. Baker, B. R. Ayres, J. O. Bash,
1194 K. Baumann, W. P. L. Carter, E. Edgerton, J. L. Fry, W. T. Hutzell, D. B. Schwede and P. B.
1195 Shepson (2015). "Modeling the Current and Future Roles of Particulate Organic Nitrates in the
1196 Southeastern United States." Environmental Science & Technology **49**(24): 14195-14203.

1197 Rollins, A. W., E. C. Browne, K. E. Min, S. E. Pusede, P. J. Wooldridge, D. R. Gentner, A. H.
1198 Goldstein, S. Liu, D. A. Day, L. M. Russell and R. C. Cohen (2012). "Evidence for NO_x Control
1199 over Nighttime SOA Formation." Science **337**(6099): 1210.

1200 Rollins, A. W., A. Kiendler-Scharr, J. L. Fry, T. Brauers, S. S. Brown, H.-P. Dorn, W. P. Dube, H.
1201 Fuchs, A. Mensah, T. F. Mentel, F. Rohrer, R. Tillmann, R. Wegener, P. J. Wooldridge and R.
1202 C. Cohen (2009). "Isoprene oxidation by nitrate radical: alkyl nitrate and secondary organic
1203 aerosol yields." Atmos. Chem. Phys. **9**: 6685-6703.

1204 Romer, P. S., K. C. Duffey, P. J. Wooldridge, H. M. Allen, B. R. Ayres, S. S. Brown, W. H.
1205 Brune, J. D. Crouse, J. de Gouw, D. C. Draper, P. A. Feiner, J. L. Fry, A. H. Goldstein, A.
1206 Koss, P. K. Misztal, T. B. Nguyen, K. Olson, A. P. Teng, P. O. Wennberg, R. J. Wild, L. Zhang
1207 and R. C. Cohen (2016). "The lifetime of nitrogen oxides in an isoprene-dominated forest."
1208 Atmos. Chem. Phys. **16**(12): 7623-7637.

1209 Saha, P. K., A. Khlystov, K. Yahya, Y. Zhang, L. Xu, N. L. Ng and A. P. Grieshop (2017).
1210 "Quantifying the volatility of organic aerosol in the southeastern US." Atmos. Chem. Phys. **17**(1):
1211 501-520.

1212 Sato, K., A. Takami, T. Iozaki, T. Hikida, A. Shimono and T. Imamura (2010). "Mass
1213 spectrometric study of secondary organic aerosol formed from the photo-oxidation of aromatic
1214 hydrocarbons." Atmospheric Environment **44**(8): 1080-1087.

1215 Schwantes, R. H., A. P. Teng, T. B. Nguyen, M. M. Coggon, J. D. Crouse, J. M. St. Clair, X.
1216 Zhang, K. A. Schilling, J. H. Seinfeld and P. O. Wennberg (2015). "Isoprene NO₃ Oxidation
1217 Products from the RO₂ + HO₂ Pathway." The Journal of Physical Chemistry A **119**(40): 10158-
1218 10171.

1219 Spracklen, D. V., J. L. Jimenez, K. S. Carslaw, D. R. Worsnop, M. J. Evans, G. W. Mann, Q.
1220 Zhang, M. R. Canagaratna, J. Allan, H. Coe, G. McFiggans, A. Rap and P. Forster (2011).

1221 "Aerosol mass spectrometer constraint on the global secondary organic aerosol budget." Atmos.
1222 Chem. Phys. **11**(23): 12109-12136.
1223 Surratt, J. D., A. W. H. Chan, N. C. Eddingsaas, M. N. Chan, C. L. Loza, A. J. Kwan, S. P.
1224 Hersey, R. C. Flagan, P. O. Wennberg and J. H. Seinfeld (2010). "Reactive intermediates
1225 revealed in secondary organic aerosol formation from isoprene." Proceedings of the National
1226 Academy of Sciences **107**(15): 6640-6645.
1227 Takegawa, N., T. Miyakawa, K. Kawamura and Y. Kondo (2007). "Contribution of Selected
1228 Dicarboxylic and ω -Oxocarboxylic Acids in Ambient Aerosol to the m/z 44 Signal of an
1229 Aerodyne Aerosol Mass Spectrometer." Aerosol Science and Technology **41**(4): 418-437.
1230 Toon, O. B., H. Maring, J. Dibb, R. Ferrare, D. J. Jacob, E. J. Jensen, Z. J. Luo, G. G. Mace, L.
1231 L. Pan, L. Pfister, K. H. Rosenlof, J. Redemann, J. S. Reid, H. B. Singh, A. M. Thompson, R.
1232 Yokelson, P. Minnis, G. Chen, K. W. Jucks and A. Pszenny (2016). "Planning, implementation,
1233 and scientific goals of the Studies of Emissions and Atmospheric Composition, Clouds and
1234 Climate Coupling by Regional Surveys (SEAC4RS) field mission." Journal of Geophysical
1235 Research: Atmospheres **121**(9): 4967-5009.
1236 Warneke, C., M. Trainer, J. A. de Gouw, D. D. Parrish, D. W. Fahey, A. R. Ravishankara, A. M.
1237 Middlebrook, C. A. Brock, J. M. Roberts, S. S. Brown, J. A. Neuman, B. M. Lerner, D. Lack, D.
1238 Law, G. Hübler, I. Pollack, S. Sjostedt, T. B. Ryerson, J. B. Gilman, J. Liao, J. Holloway, J.
1239 Peischl, J. B. Nowak, K. C. Aikin, K. E. Min, R. A. Washenfelder, M. G. Graus, M. Richardson,
1240 M. Z. Markovic, N. L. Wagner, A. Welti, P. R. Veres, P. Edwards, J. P. Schwarz, T. Gordon, W.
1241 P. Dube, S. A. McKeen, J. Brioude, R. Ahmadov, A. Bougiatioti, J. J. Lin, A. Nenes, G. M.
1242 Wolfe, T. F. Hanisco, B. H. Lee, F. D. Lopez-Hilfiker, J. A. Thornton, F. N. Keutsch, J. Kaiser, J.
1243 Mao and C. D. Hatch (2016). "Instrumentation and measurement strategy for the NOAA SENEX
1244 aircraft campaign as part of the Southeast Atmosphere Study 2013." Atmos. Meas. Tech. **9**(7):
1245 3063-3093.
1246 Wilson, J. C., B. G. Lafleu, H. Hilbert, W. R. Seebaugh, J. Fox, D. W. Gesler, C. A. Brock, B. J.
1247 Huebert and J. Mullen (2004). "Function and Performance of a Low Turbulence Inlet for
1248 Sampling Supermicron Particles from Aircraft Platforms." Aerosol Science and Technology
1249 **38**(8): 790-802.
1250 Worton, D. R., J. D. Surratt, B. W. LaFranchi, A. W. H. Chan, Y. Zhao, R. J. Weber, J.-H. Park,
1251 J. B. Gilman, J. de Gouw, C. Park, G. Schade, M. Beaver, J. M. S. Clair, J. Crouse, P.
1252 Wennberg, G. M. Wolfe, S. Harrold, J. A. Thornton, D. K. Farmer, K. S. Docherty, M. J.
1253 Cubison, J.-L. Jimenez, A. A. Frossard, L. M. Russell, K. Kristensen, M. Glasius, J. Mao, X.
1254 Ren, W. Brune, E. C. Browne, S. E. Pusede, R. C. Cohen, J. H. Seinfeld and A. H. Goldstein
1255 (2013). "Observational Insights into Aerosol Formation from Isoprene." Environmental Science
1256 & Technology **47**(20): 11403-11413.
1257 Xie, Y., F. Paulot, W. P. L. Carter, C. G. Nolte, D. J. Luecken, W. T. Hutzell, P. O. Wennberg, R.
1258 C. Cohen and R. W. Pinder (2013). "Understanding the impact of recent advances in isoprene
1259 photooxidation on simulations of regional air quality." Atmos. Chem. Phys. **13**(16): 8439-8455.
1260 Xu, L., S. Suresh, H. Guo, R. J. Weber and N. L. Ng (2015). "Aerosol characterization over the
1261 southeastern United States using high-resolution aerosol mass spectrometry: spatial and
1262 seasonal variation of aerosol composition and sources with a focus on organic nitrates." Atmos.
1263 Chem. Phys. **15**(13): 7307-7336.
1264 Zhang, H., L. D. Yee, B. H. Lee, M. P. Curtis, D. R. Worton, G. Isaacman-VanWertz, J. H.
1265 Offenberg, M. Lewandowski, T. E. Kleindienst, M. R. Beaver, A. L. Holder, W. A. Lonneman, K.
1266 S. Docherty, M. Jaoui, H. O. T. Pye, W. Hu, D. A. Day, P. Campuzano-Jost, J. L. Jimenez, H.
1267 Guo, R. J. Weber, J. de Gouw, A. R. Koss, E. S. Edgerton, W. Brune, C. Mohr, F. D. Lopez-
1268 Hilfiker, A. Lutz, N. M. Kreisberg, S. R. Spielman, S. V. Hering, K. R. Wilson, J. A. Thornton and
1269 A. H. Goldstein (2018). "Monoterpenes are the largest source of summertime organic aerosol in
1270 the southeastern United States." Proceedings of the National Academy of Sciences **115**(9):
1271 2038.

1272 Zhang, Q., M. R. Alfarra, D. R. Worsnop, J. D. Allan, H. Coe, M. R. Canagaratna and J. L.
1273 Jimenez (2005). "Deconvolution and Quantification of Hydrocarbon-like and Oxygenated
1274 Organic Aerosols Based on Aerosol Mass Spectrometry." Environmental Science & Technology
1275 **39**(13): 4938-4952.

1276 Zhang, Q., J. L. Jimenez, M. R. Canagaratna, J. D. Allan, H. Coe, I. Ulbrich, M. R. Alfarra, A.
1277 Takami, A. M. Middlebrook, Y. L. Sun, K. Dzepina, E. Dunlea, K. Docherty, P. F. DeCarlo, D.
1278 Salcedo, T. Onasch, J. T. Jayne, T. Miyoshi, A. Shimono, S. Hatakeyama, N. Takegawa, Y.
1279 Kondo, J. Schneider, F. Drewnick, S. Borrmann, S. Weimer, K. Demerjian, P. Williams, K.
1280 Bower, R. Bahreini, L. Cottrell, R. J. Griffin, J. Rautiainen, J. Y. Sun, Y. M. Zhang and D. R.
1281 Worsnop (2007). "Ubiquity and dominance of oxygenated species in organic aerosols in
1282 anthropogenically-influenced Northern Hemisphere midlatitudes." Geophysical Research Letters
1283 **34**(13): L13801.

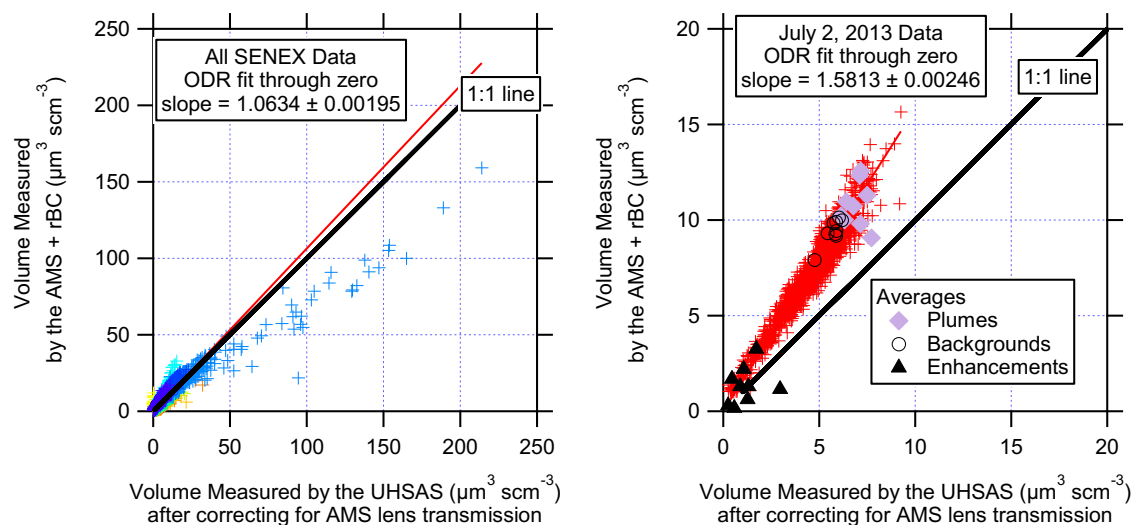
1284 Zhang, Q., C. O. Stanier, M. R. Canagaratna, J. T. Jayne, D. R. Worsnop, S. N. Pandis and J.
1285 L. Jimenez (2004). "Insights into the Chemistry of New Particle Formation and Growth Events in
1286 Pittsburgh Based on Aerosol Mass Spectrometry." Environmental Science & Technology **38**(18):
1287 4797-4809.

1288 Zheng, Y., N. Unger, A. Hodzic, L. Emmons, C. Knote, S. Tilmes, J. F. Lamarque and P. Yu
1289 (2015). "Limited effect of anthropogenic nitrogen oxides on secondary organic aerosol
1290 formation." Atmos. Chem. Phys. **15**(23): 13487-13506.

1291
1292
1293

1294 Supplemental Information

1295 In the main text, we noted a discrepancy between overall average aerosol volume estimates
1296 based on size measurements vs. AMS for the flight analyzed here (see Figure S1). We checked
1297 to see if this bias was also present in the individual plumes studied here by calculating the
1298 volume changes from the sizing instruments and the derived volume changes from the
1299 AMS+rBC mass. There is quite a bit of scatter in the volume enhancements, with most of the
1300 points falling along the same line as the data for this flight. It is unclear why the two types of
1301 volume measurements disagree more for this flight. Therefore, the bias in volume changes
1302 introduces additional uncertainty in the magnitude of the plume enhancements.
1303



1304
1305 **Figure S1.** Aerosol volume measured using the total aerosol mass from the AMS plus refractory
1306 black carbon (rBC) and mass-weighted densities versus the aerosol volume measured by
1307 optical size with the UHSAS after correcting for AMS lens transmission. The procedure for
1308 calculating the mass-weighted density is described by Bahreini et al. (2009). On average, the
1309 measured aerosol volume from composition is roughly equal to the measured aerosol volume
1310 from size for the entire SENEX study (left hand panel) and is higher than one for the flight
1311 analyzed here (July 2, 2013, right hand panel).
1312

1313 Corrections for AMS UMR nitrate data and applicability to pRONO₂ estimation

1314
1315 Nitrate in the AMS is quantified in unit mass resolution mode (UMR) as the sum of the estimated
1316 NO⁺ at *m/z* 30 and NO₂⁺ at *m/z* 46, with a correction factor to account for the smaller ions (N⁺
1317 and HNO₃⁺, mostly) produced from nitrate (Allan et al., 2004). The default AMS UMR
1318 quantification algorithm (documented in the AMS “fragmentation table”) estimates NO⁺ as the
1319 total signal at *m/z* 30 minus a small (2.2% of OA at *m/z* 29, “Org29” in AMS parlance)
1320 subtraction to account for organic interferences and an isotopic correction for naturally-occurring
1321 ¹⁵N₂ from nitrogen in air. The default UMR fragmentation table was developed for mixed ambient
1322 aerosols, in particular in urban studies, and it is the responsibility of each AMS user to correct it
1323 as needed for each study. In environments with high biogenic contributions to total OA, and/or
1324 low total nitrate concentrations, the contribution of the CH₂O⁺ ion can be much larger than the

1325 default subtraction at m/z 30. Similarly, the CH_2O_2^+ ion at m/z 46 becomes non-negligible, and
1326 hence nitrate reported from AMS data with UMR resolution will frequently be overestimated in
1327 these situations. The poor performance of the default AMS correction is likely due to the initial
1328 focus on urban OA with high nitrate fractions when deriving those corrections (Allan et al., 2004,
1329 Zhang et al., 2004).

1330
1331 Here we derive a set of corrections based on an aircraft high-resolution (HR) dataset acquired
1332 with the University of Colorado HR-AMS (Dunlea et al., 2009) on the NASA DC-8 during the
1333 SEAC⁴RS campaign (Toon et al., 2016). SEAC⁴RS took place with a strong emphasis on the
1334 SEUS 6 weeks after the SENEX flight analyzed in this manuscript. Based on an initial screening
1335 of the correlations of the CH_2O^+ and CH_2O_2^+ ions with UMR signals, 10 potential UMR m/z
1336 between m/z 29 and m/z 53 were selected as viable for deriving suitable corrections. Further
1337 analysis using three specific SEAC⁴RS flights (RF11 on 30 Aug 30th, 2013, RF16 on Sep 11th,
1338 2013 and RF18 on Sep 16th, 2013) that covered a wide range of OA composition with both
1339 strong biogenic contributions and fresh and aged biomass plumes showed that only four m/z
1340 (29, 42, 43 and 45) had good enough S/N and robust enough correlations to be used as
1341 corrections. Table S1 summarizes the correction coefficients obtained in this analysis, and
1342 Figure S2 shows the ability of matching the actual NO^+ and NO_2^+ signals (as obtained from
1343 high-resolution analysis of these flights) with the corrected UMR procedure. These corrections
1344 are applied as:

$$\text{UMR NO} = \text{Signal}(m/z30) - a_i * \text{Signal}(\text{Variable}_i)$$

$$\text{UMR NO}_2 = \text{Signal}(m/z 46) - b_i * \text{Signal}(\text{Variable}_i)$$

1348
1349 with the coefficients a_i and b_i as reported in Table S1. It should be noted that in all cases the
1350 contributions of C^{18}O^+ to m/z 30 need to be subtracted first before applying the correction (which
1351 is constrained to the organic CO_2^+ signal, measured at m/z 44, by the naturally-occurring
1352 isotopic ratio and assuming that OA produces $\text{CO}^+ = \text{CO}_2^+$ (Zhang et al., 2005, Takegawa et al.,
1353 2007). Likewise, the contribution of $^{13}\text{CO}^+$ to Org29 needs to be subtracted first. It is hence very
1354 important for this analysis that the corrections to the AMS frag table to suitably estimate the
1355 contribution of gas phase CO_2^+ to total UMR m/z 44 as well as the baseline correction for m/z 29
1356 be properly applied first (Allan et al., 2004). Finally, also note that the corrections using m/z 29
1357 and 43 are rather based on Org29 and Org43, which are standard AMS products that take the
1358 OA relative ionization efficiency (RIE) into account.

1359
1360 For the SEAC⁴RS dataset, the corrections amounted to on average subtracting 55% from UMR
1361 m/z 30 and 33% from UMR m/z 46. Despite this large subtraction, the corrected data correlates
1362 very well with the HR AMS results, with less than 5% deviation in the regression slope between
1363 the two datasets.

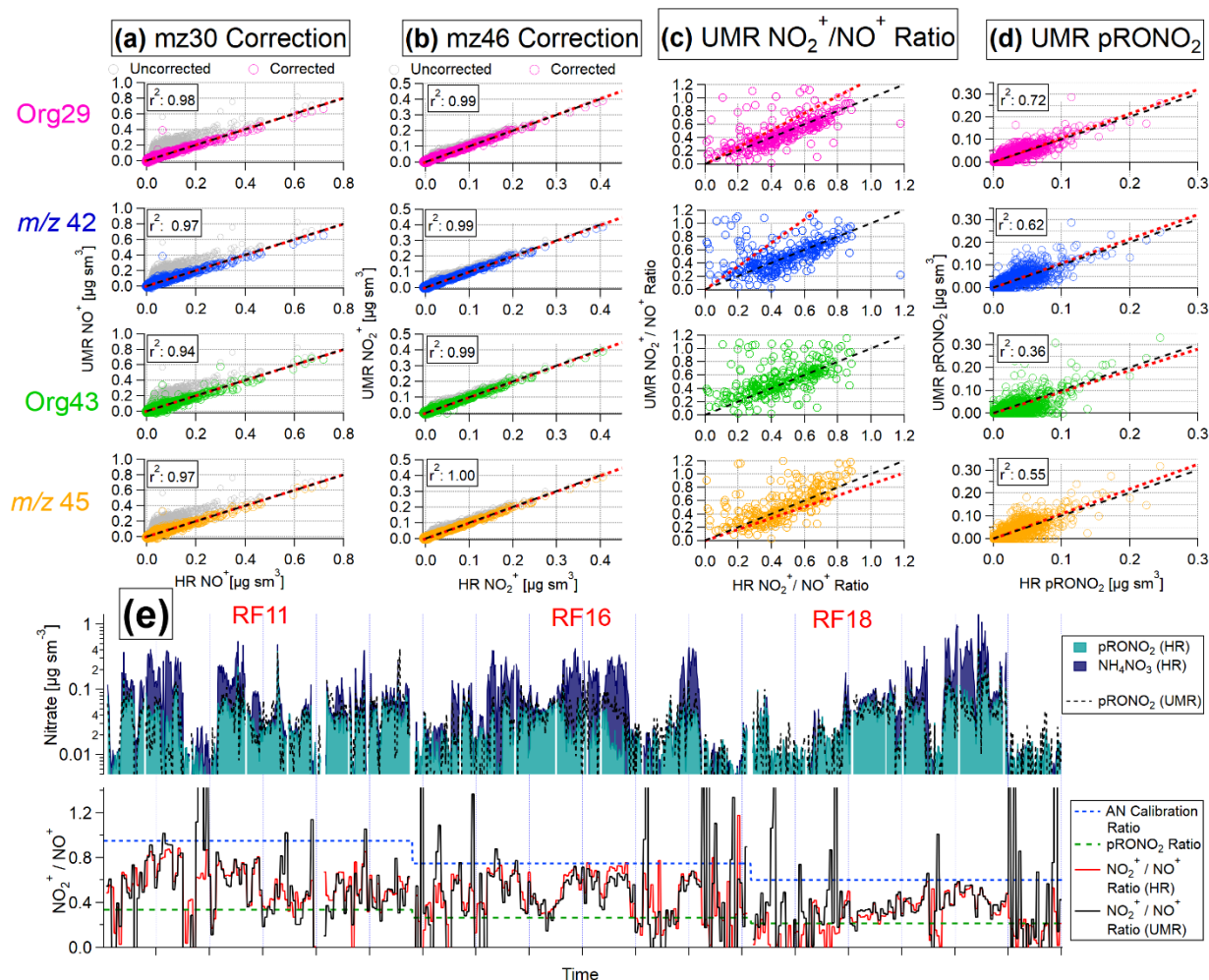
1364
1365 Although all of the corrections in Table S1 were valid for the SEAC⁴RS data set, for the flight
1366 analyzed here we chose Org29 to correct m/z 30 and mz 45 correction to correct m/z 46
1367 because they were the closest organic signals to the UMR nitrate peaks with organic
1368 interferences and may be more valid for other field studies where different types of OA are

1369 sampled. After these UMR signals were corrected and the appropriate RIEs and CE were
1370 applied, the nitrate mass concentrations in the final data archive for the flight analyzed here
1371 were reduced by 0-0.24 $\mu\text{g sm}^{-3}$, averaging 0.11 $\mu\text{g sm}^{-3}$ or 32%. The corresponding increase in
1372 OA due to the organic interferences in the UMR nitrate had linear dependence on the reported
1373 OA mass concentrations ($r^2 = 0.89$) with a slope of 1.3%.

1374
1375 To estimate the fraction of nitrate that is organic nitrate (pRONO₂) the use of the NO₂⁺/NO⁺ ratio
1376 with an empirically determined pRONO₂ calibration ratio has been successfully used previously
1377 with HR-AMS data (Farmer et al., 2010, Fry et al., 2013, Ayres et al., 2015, Fisher et al., 2016,
1378 Lee et al., 2016, Day et al., 2017, Palm et al., 2017). Figure S2 summarizes how well the ratio of
1379 the corrected UMR *m/z* 30 and 46 signals correlate with the NO₂⁺ and NO⁺ (and ratios)
1380 determined using HR data. As expected, there is considerable scatter at very low nitrate
1381 concentrations (which is a considerable part of the dataset, as the time series shows, since the
1382 free troposphere was sampled extensively). However, for the predicted pRONO₂ (which is
1383 mass-weighted), most of this scatter disappears, and for concentrations above 0.1 $\mu\text{g sm}^{-3}$ of
1384 nitrate there is good agreement between the HR results and the UMR-corrected pRONO₂,
1385 regardless of the correction chosen. For lower concentrations the scatter is considerable larger,
1386 with the Org29 correction providing the best overall agreement. Based on the variability in this
1387 dataset for this correction (Org29), we estimate the uncertainty in pRONO₂ fraction
1388 apportionment using UMR to be about 30%, in addition to an estimated uncertainty for the
1389 apportionment method using HR of 20%. From the comparison of UMR-corrected total nitrate
1390 to HR nitrate (not shown), we estimate an additional error of 5% for total nitrate error using
1391 these corrections.

1392
1393 As mentioned in the main text, the empirically determined pRONO₂ calibration ratio used for the
1394 flight data analyzed here was the ratio of NO₂⁺/NO⁺ from the ammonium nitrate calibration
1395 aerosols divided by 2.8. This factor was determined as the average of several literature studies
1396 (Fry et al., 2009, Rollins et al., 2009, Farmer et al., 2010, Sato et al., 2010, Fry et al., 2011,
1397 Boyd et al., 2015) and applied according to the “ratio of ratios” method (Fry et al., 2013). The
1398 ammonium nitrate NO₂⁺/NO⁺ ratio was obtained from the two calibrations on 30 June and 7 July
1399 that bracketed the flight on 2 July, as described above. This ratio averaged 0.490. Hence, the
1400 organic nitrate NO₂⁺/NO⁺ ratio was estimated to be 0.175. The ratio of NO₂⁺/NO⁺ from the flight
1401 data was then used with the pRONO₂ and ammonium nitrate NO₂⁺/NO⁺ calibration ratios to
1402 estimate the fraction of the total corrected nitrate mass concentrations that was organic
1403 (pRONO₂) or inorganic (nitrate associated with ammonium or NH₄NO₃). Propagating the 30%
1404 UMR vs HR uncertainty and 20% apportionment (see above) error on top of the 34% AMS total
1405 nitrate measurement uncertainty results in $\pm 50\%$ uncertainties in the derived organic nitrate
1406 mass concentrations (and similar for NH₄NO₃; however it will depend on the relative
1407 contributions of pRONO₂ and NH₄NO₃ to total nitrate since the absolute concentration errors
1408 associated with pRONO₂ - NH₄NO₃ apportionment should be similar [64]).

1409

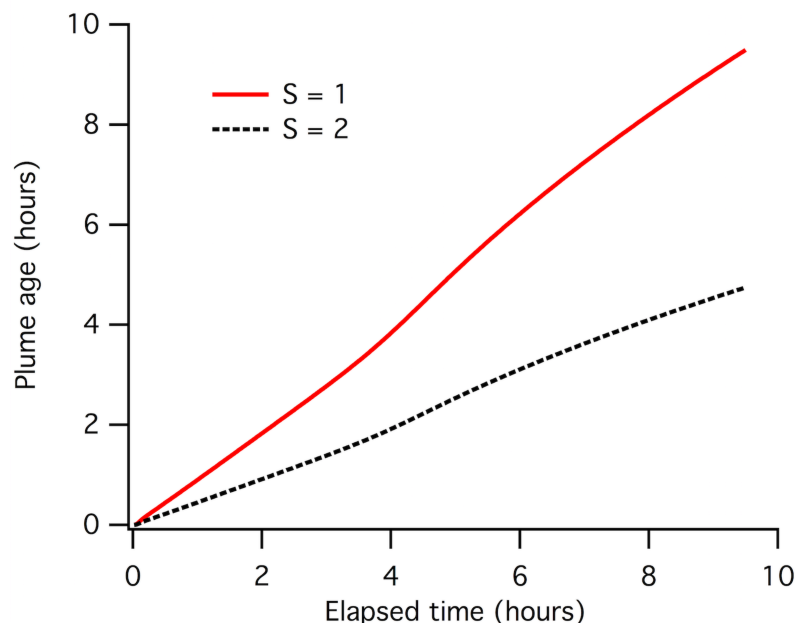


1410
 1411 **Figure S2.** (a and b) Comparison of m/z 30 and 46 with the NO^+ and NO_2^+ signals from the high
 1412 resolution analysis of the AMS data before and after applying the four different corrections listed
 1413 in Table S1. The Pearson r^2 for the corrected dataset is shown as well. (c) Comparison of the
 1414 $\text{NO}_2^+/\text{NO}^+$ ratio obtained from HR analysis with the ratios of the corrected UMR NO and NO_2
 1415 variables (d) Comparison of the pRONO_2 concentrations derived using the HR and UMR $\text{NO}_2^+/\text{NO}^+$
 1416 ratios. (e) Time series of the total and speciated nitrate as reported from HR analysis of the
 1417 SEAC⁴RS data (NASA 2018)(NASA 2018)(NASA 2018)(NASA 2018)(NASA 2018)(DOI:
 1418 10.5067/Aircraft/SEAC4RS/Aerosol-TraceGas-Cloud) compared to the speciation using the
 1419 Org29 correction (note the logarithmic scale). The bottom time series shows the $\text{NO}_2^+/\text{NO}^+$ ratio
 1420 that the speciation is based on, again for the HR and corrected UMR case.

1421 **Table S1.** Coefficients used to correct m/z 30 and 46 to estimate total nitrate.

AMS Variable	Correction coefficient for m/z 30 (a _i)	Correction coefficient for m/z 46 (b _i)
Org29	0.215	0.037
m/z 42	0.51	0.092
Org43	0.215	0.037
m/z 45	0.72	0.127

1422



1423

1424

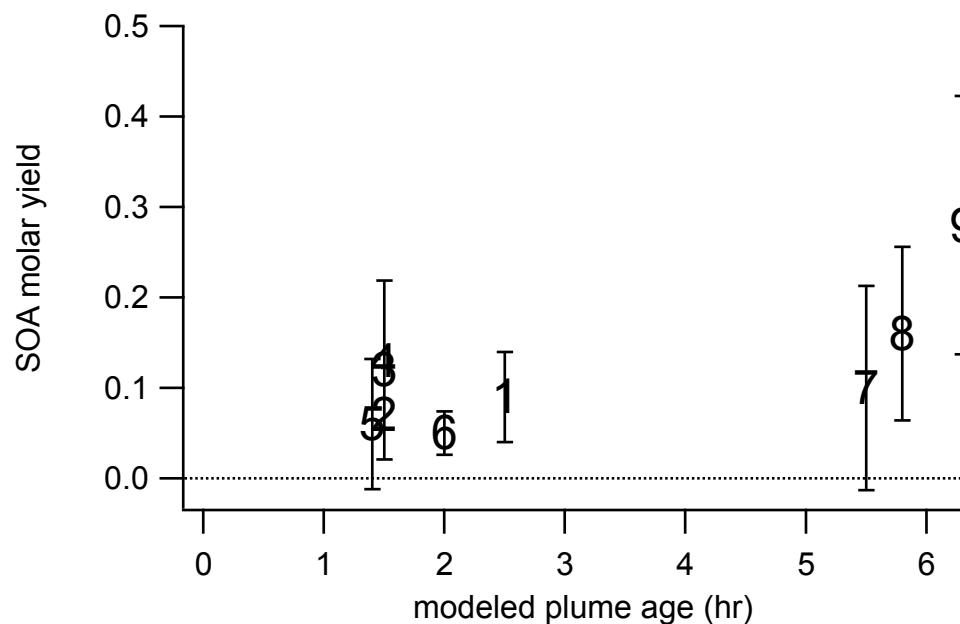
1425

1426

1427

1428

Figure S3. Calculated plume age vs. elapsed time in a box model run for a single representative night. Plume ages on the y-axis are calculated based on Equation 1 in the main text but using model NO₂ and O₃ data. Time since sunset on the x-axis is the model elapsed time (i.e., run time of the model during darkness).



1429

1430

1431

1432

1433

Figure S4. SOA molar yield is positively correlated with estimated plume age. This SOA molar yield is based on Eq. 3, with error bars determined by propagation of observed variability in pRONO₂ and isoprene, where multiple point averaging was possible. Markers correspond to

1434 plume numbers.). Based on the box model described in more detail below, the first-generation
1435 isoprene products peak at a approximately 4 hours plume age and then begin to decay.

1436

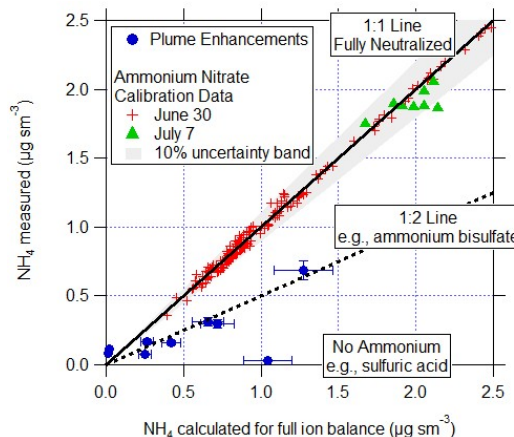
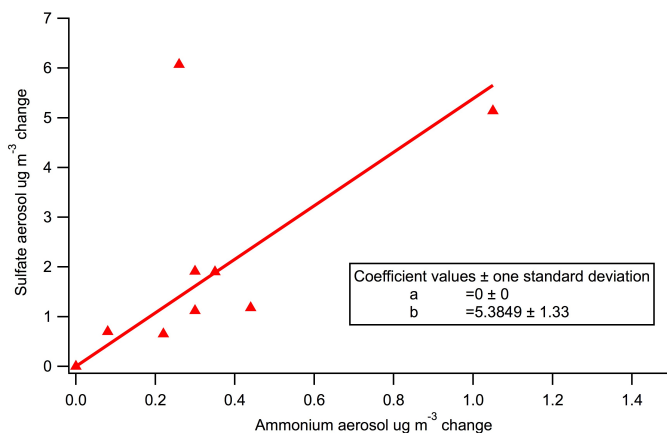
1437 **Table S2.** Peak ambient (wet) aerosol surface area during each plume used in the yield
1438 analysis (plume numbers 1 – 9), and for the two longer urban plumes transected at the end of
1439 the flight.

plume number	7/2/13 plume time (UTC)	Peak aerosol surface area ($\mu\text{m}^2 \text{cm}^{-3}$)
1	2:18	280
2	2:20	370
3	2:21	470
4	3:03	340
5	3:55	800
6	4:34	470
7	4:37	370
8	4:39	420
9	5:04	490
Urban plume	5:36	340
Urban plume	6:37	300

1440

1441

1442



1443
 1444
 1445
 1446
 1447
 1448
 1449
 1450
 1451
 1452
 1453
 1454
 1455
 1456
 1457
 1458
 1459

Figure S5. (a) In-plume change in sulfate mass concentration vs. change in ammonium aerosol mass concentration is generally well correlated, with a slope of 5.4. The masses of the cations and anions would give an ion balance for pure $(\text{NH}_4)_2\text{SO}_4$ of $\text{MW}(\text{SO}_4)/(2 \times \text{MW}(\text{NH}_4)) = 2.7$, and for $(\text{NH}_4)\text{HSO}_4$ of $\text{MW}(\text{SO}_4)/(\text{MW}(\text{NH}_4)) = 5.4$. Hence, this slope provides support for a mix of these two ammonium sulfate salts, with sometimes exclusively $(\text{NH}_4)\text{HSO}_4$. This is consistent with incomplete neutralization of the sulfate mass by ammonium. The one clear outlier (sulfate increase of $6 \mu\text{g m}^{-3}$ for Plume #5) suggests excess sulfate, rendering ammonium or other inorganic nitrate formation even less likely. Points with ammonium aerosol below $0.1 \mu\text{g m}^{-3}$ are within the variability of that measurement; their omission does not change the slope. (b) Measured vs. calculated (ion balanced) NH_4 for calibration data and plume enhancements. This also shows that plumes are acidic than ammonium sulfate, ruling out the possibility of inorganic nitrate formation.

1460 **Additional AMS and auxiliary data from plumes**

1461

1462 **Table S3.** Additional information for the list of plumes used in this NO₃ + isoprene SOA yield
 1463 analysis, for which key yield-related data is presented in Table 1. For each plume, the delta-
 1464 values listed indicate the difference between in-plume and outside-plume background in
 1465 average observed concentration. After each plume number, the numbers of points averaged for
 1466 isoprene and AMS, respectively, are listed. Plume numbers annotated with * indicate brief
 1467 plumes for which only single-point measurements of in-plume aerosol composition were
 1468 possible. Also shown are the plume changes in isoprene used in the present analysis (Δ isop,
 1469 the difference between in-plume and background isoprene concentration, reproduced from
 1470 Table 1), alongside for comparison the Δ isop determined as the difference between in-plume
 1471 isoprene and the modeled sunset (initial) concentration of isoprene present at that location
 1472 outside of the plume, determined using an iterative box model (Edwards et al., 2017). The
 1473 similarity between these two values for most points suggests that the isoprene just outside of
 1474 each plume transect was largely unperturbed from the sunset initial value.

plume number [#isop/#AMS]	7/2/13 plume time (UTC)	Δ ORG _{aero} ($\mu\text{g m}^{-3}$)	Δ NH _{4,aero} ($\mu\text{g m}^{-3}$)	Δ SO _{4,aero} ($\mu\text{g m}^{-3}$)	Temp (C)	%RH	Δ isop (pptv)	Δ isop from model (pptv)	Isop:M' Mole Rat
Typical variability ($\mu\text{g m}^{-3}$):		0.75	0.1	0.5					
1 [2/3]	2:18	0.35	0	0	23.6	66.5	-335	-327	36.5
2 [*]	2:20	0.89	0.3	1.91	23.6	65	-404	-453	71.4
3 [4/5]	2:21	1.25	1.05	5.14	23.6	65.2	-228	-337	16.6
4 [*]	3:03	0.16	0.08	0.7	21.2	68.1	-453	-391	50.6
5 [3/4]	3:55	0.32	0.26	6.07	21.9	65.5	-255	-376	34.2
6 [2/2]	4:34	0.57	0.3	1.12	19.9	74.6	-713	-233	17.3
7 [5/6]	4:37	1.05	0.22	0.65	19.7	76.2	-298	-221	14.2
8 [2/3]	4:39	1.26	0.44	1.18	18.3	82.2	-443	-353	11.0
9 [7/8]	5:04	1.45	0.35	1.9	17.2	84.8	-293	-434	17.8

1475

1476

1477

1478 **Box model calculations**

1479 Box model simulations were performed using the Dynamically Simple Model of Atmospheric
 1480 Chemical Complexity (DSMACC, [http://wiki.seas.harvard.edu/geos-](http://wiki.seas.harvard.edu/geos-chem/index.php/DSMACC_chemical_box_model)
 1481 [chem/index.php/DSMACC_chemical_box_model](http://wiki.seas.harvard.edu/geos-chem/index.php/DSMACC_chemical_box_model)), containing the Master Chemical Mechanism
 1482 v3.3.1 chemistry scheme (<http://mcm.leeds.ac.uk/MCM/>). The model approach is similar to that
 1483 described in detail in Edwards et al. 2017, and the accompanying supplement, with the model
 1484 run over a 9.5 hour night to simulate the nocturnal residual layer. For the nocturnal simulation
 1485 used in this work (for both the plume lifetime calculation and the peroxy radical lifetime analysis
 1486 in Sect. 4.3) the model was initialized with concentrations of the constraining species
 1487 representative of the SENEX observations (Table S4). As the model is simulating power plant
 1488 plume evolution from point of emission, a starting NO mixing ratio of 10 ppb was used to
 1489 constrain NO_x, and the chemistry scheme was subsequently allowed to partition the reactive
 1490 nitrogen. The top panels in Figure S7 show the evolution of key species during this nocturnal
 1491 simulation.

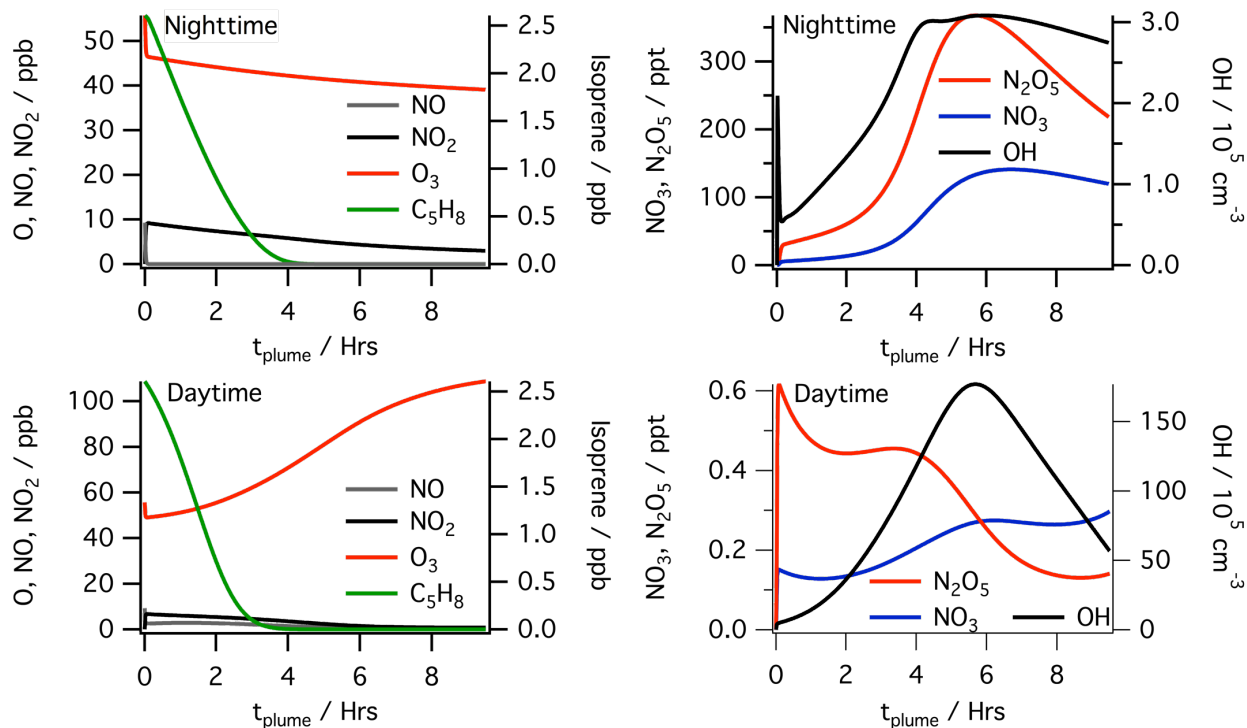
1492 **Table S4:** Species constrained (MCM v3.3.1 names) during model simulations and constraining
 1493 values. Constraint column indicates if species concentrations were held at the constrained value
 1494 throughout the simulation (Fixed) or allowed to vary after initialization (Initial).

Species	Mixing ratio	Units	Constraint
NO	9.28	ppb	Initial
O3	55.72	ppb	Initial
CO	134.00	ppb	Fixed
CH4	1920.00	ppb	Fixed
C5H8	2606.80	ppt	Initial
APINENE	38.87	ppt	Initial
BPINENE	195.50	ppt	Initial
LIMONENE	12.42	ppt	Initial
MACR	454.13	ppt	Initial
MVK	1006.00	ppt	Initial
IC4H10	47.00	ppt	Fixed
NC4H10	128.00	ppt	Fixed
C2H6	1199.00	ppt	Fixed
C2H4	117.00	ppt	Fixed
C2H2	145.00	ppt	Fixed
NC6H14	20.00	ppt	Fixed
IC5H12	120.00	ppt	Fixed
NC5H12	76.00	ppt	Fixed
C3H8	344.00	ppt	Fixed
C3H6	26.00	ppt	Fixed
CH3COCH3	2556.00	ppt	Fixed
BENZENE	35.90	ppt	Fixed
C2H5OH	2239.00	ppt	Fixed
MEK	309.00	ppt	Fixed
CH3OH	5560.00	ppt	Fixed

1495 The daytime simulation used for comparison in Sect. 4.3 of the main manuscript (lower panels
 1496 of Figure S7) uses the same initialization as the nocturnal simulation; with the only difference
 1497 being the model is run during the daytime. Photolysis rates are calculated using TUV
 1498 (<https://www2.acom.ucar.edu/modeling/tropospheric-ultraviolet-and-visible-tuv-radiation-model>).
 1499 The daytime simulation does not accurately simulate daytime mixing ratios of species such as
 1500 O₃ representative of SENEX observations. However, the intent of this simulation is to compare
 1501 model daytime peroxy radical fate and lifetime with the nocturnal simulation. The presence of

1502 intense convective mixing in the daytime planetary boundary layer of the Southeast US makes
1503 accurately modeling these concentrations difficult with a zero dimensional model.

1504



1505

1506 **Fig. S6.** Model calculated NO, NO₂, O₃, and isoprene (left) and NO₃, N₂O₅ and OH (right for the
1507 nocturnal (top) and daytime (bottom) simulations shown in Sect. 4.3.

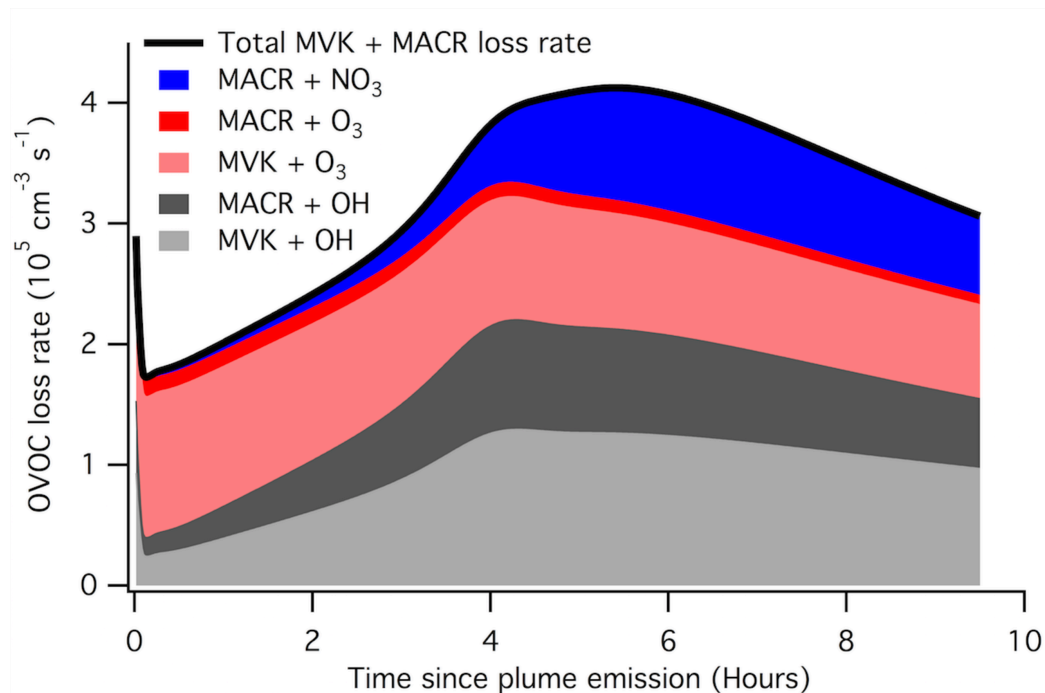
1508

1509 Additional considerations investigated via RO₂ fate box modeling

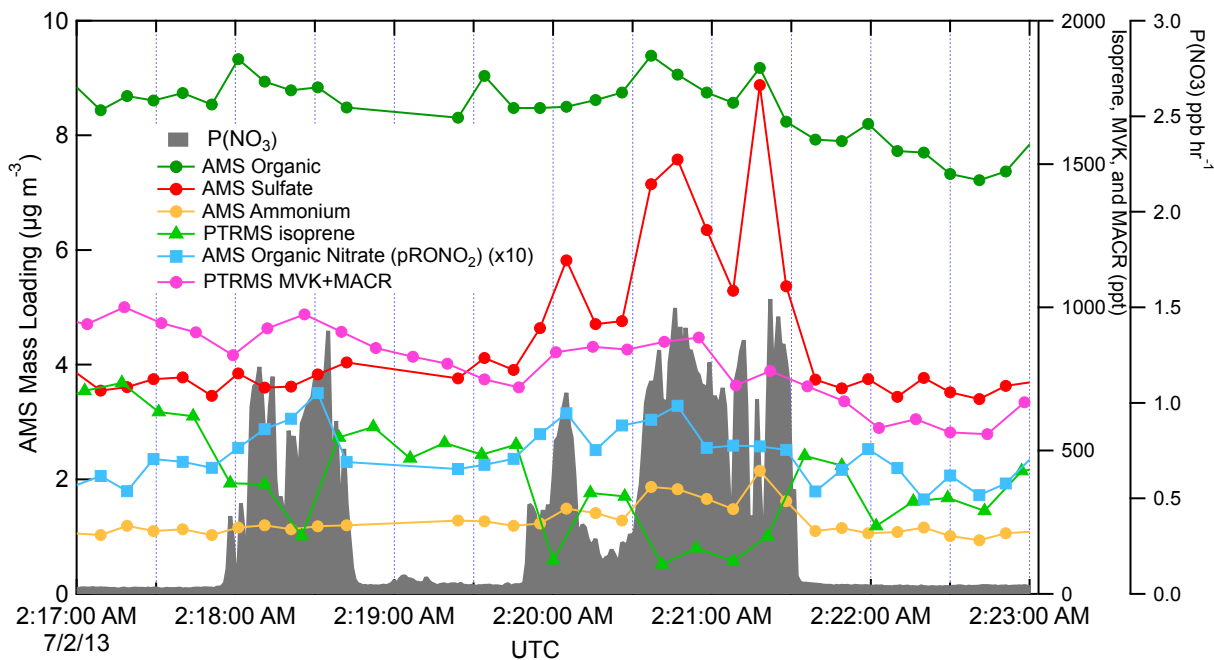
1510

1511 Based on the potentially larger than previously estimated contribution of RO₂+RO₂ reactions at
1512 night, we considered a related possible source of a high bias in the determined SOA yields. If
1513 NO₃ reaction with the major daytime isoprene oxidation products MVK and/or MACR produces
1514 RO₂ radicals that can cross-react with NO₃ + isoprene products to produce condensable
1515 products, this would be a mechanism of recruiting isoprene-derived organic mass into the
1516 aerosol, but that original isoprene oxidation would not be counted in the denominator of the yield
1517 calculation, since its interaction with NO₃ began as MACR or MVK. In the box model, substantial
1518 MVK and MACR are available in the plume at nighttime, but only MACR reacts with NO₃, and a
1519 maximum fraction of one-quarter of MVK+MACR losses go to reaction with NO₃ overnight (see
1520 Figure S8). In addition, in our power plant plume observations, MVK+MACR are not observed to
1521 be appreciably depleted by the large NO₃ injection, further suggesting that this chemistry is not
1522 a substantial additional source of SOA (see Figure S9).

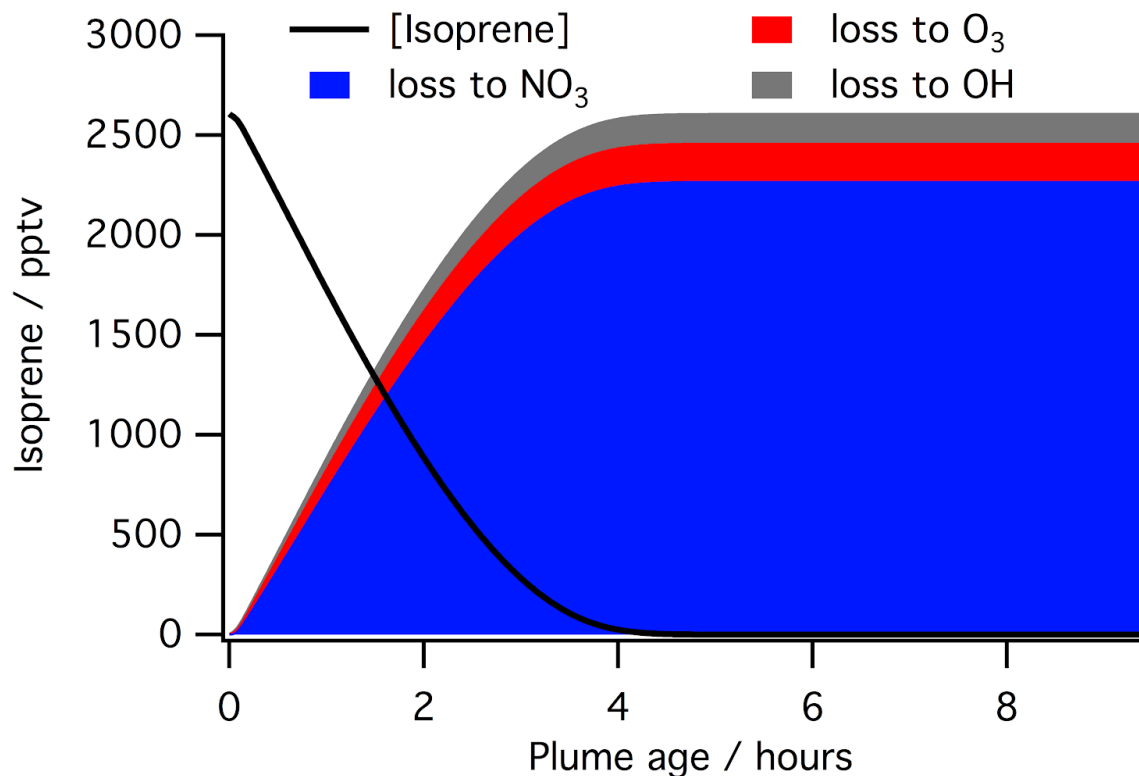
1523



1524
 1525 **Figure S7.** Calculated (via MCM) loss rate contributions for the daytime isoprene products
 1526 methyl vinyl ketone (MVK) and methacrolein (MACR) in the simulated nighttime plume used in
 1527 the text. Only MACR reacts with NO_3 , and the contribution of this process to total losses (green
 1528 stack) is relatively minor.



1529
 1530 **Figure S8.** MVK and MACR are not titrated on the timescale of these yield estimates in power
 1531 plant plumes.
 1532



1533
1534
1535
1536
1537
1538

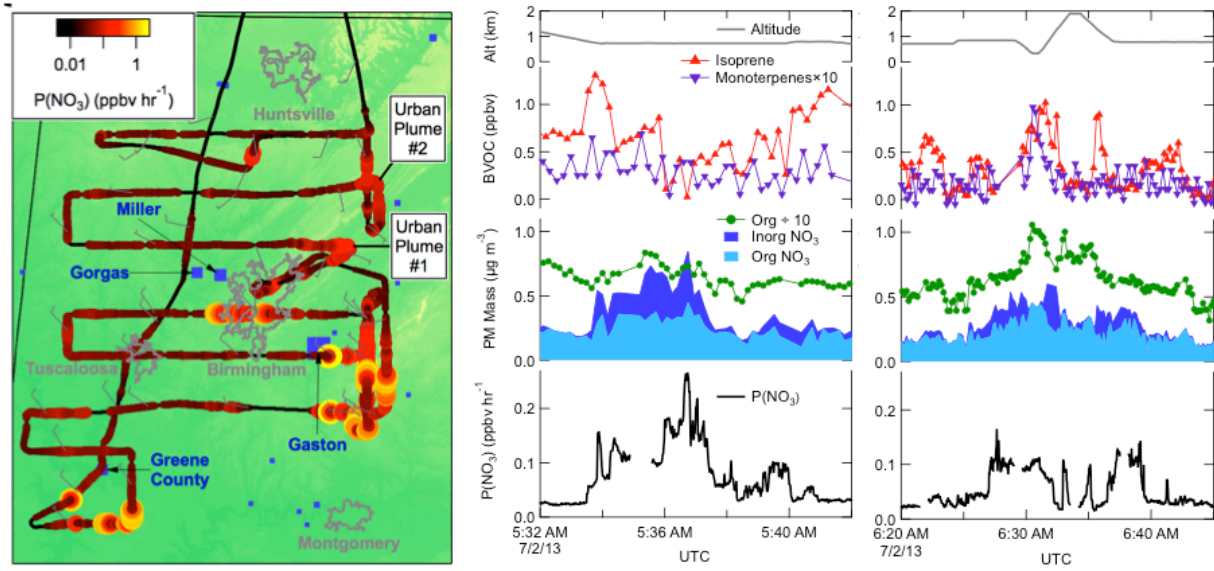
Figure S9. Model simulation of typical in-plume consumption of isoprene (black line), and stacked plot showing the contributions to this from the NO₃, O₃, and OH. Modeled plume was emitted at sunset, so this represents nocturnal processing under power plant plume conditions.

1539 **Two urban plume case studies**

1540

1541 In addition to the nine power plant plumes analyzed above to determine the NO₃ + isoprene
1542 SOA molar yield, towards the end of the July 2 flight, the Birmingham urban plume was
1543 intercepted twice (around 5:36 am and 6:37 am UTC, Fig. 8). These downwind urban plumes
1544 are among the most aged plumes (estimated at 5.2 and 5.8 hours, respectively), but are also
1545 substantially more diffuse than the narrow power plant plume intercepts and have lower peak
1546 *P*(NO₃). Nevertheless, we note that these two plumes contain periods of apparent anti-
1547 correlation of isoprene and organic nitrate aerosol time series and high apparent SOA molar
1548 yields (23%, 19%) and mass yields (62%, 51%), if calculated by the same method as above and
1549 omitting the period of vertical profiling in the second plume. Potentially complicating these urban
1550 SOA yield determinations is the fact that the inorganic fraction of nitrate was much larger than in
1551 the power plant plumes (see Fig. 8). The background isoprene is also somewhat lower in these
1552 urban plumes, potentially shifting the NO₃/N₂O₅ fate to reactions other than NO₃ + isoprene (see
1553 Fig. S4 in Edwards et al. (Edwards et al., 2017)). The aerosol surface area is not noticeably
1554 higher in these urban plumes, which one might expect to lead to a larger contribution of N₂O₅
1555 uptake and hydrolysis. In the more complex mix of gases characteristic of an urban plume, we
1556 hesitate to attribute these apparent yields exclusively to the NO₃ + isoprene reaction.

1557



1558
1559
1560
1561
1562
1563
1564
1565

Figure S10. Flight map and time series of two urban plume intercepts, showing anticorrelation of organic nitrate and isoprene. These more diffuse plumes, with lower $P(\text{NO}_3)$ and larger inorganic nitrate contribution, make yield determination more uncertain, so we do not include them in the overall yield determination. However, using the same methodology as for the power plant plumes would give similarly high yields for these very aged plumes.